sequence of rat Sox6, AC119630. mRNA sequence of human SOX6, NM_033326; mRNA sequence of mouse Sox6, AK030713; mRNA sequence of mouse Sox9, NM_011448.

Results and discussion

Determination of the human embryonic SOX6 promoter

We identified the transcription start region of the human and mouse Sox6 genes by 5′ RACE analysis (Figs. 1A and B). A comparison with the genomic sequence revealed that there were two non-coding exons in the human and mouse Sox6 genes. The identified transcription start regions were located approximately 260 kbp apart from the start codon (at exon 3) in humans and 230 kbp in mice (Fig. 1B). The size of each exon, their intervals, and coding exons were similar between the two species [18]. The identified Sox6 cDNA partially overlapped with a previously identified clone (GenBank Accession No. AK030713), with our clone being approximately 500-bp longer. The identified promoter lacked the TATA box, instead containing a GC rich sequence. We performed a BLAST search using the human genomic sequence around the identified transcriptional start region (between 3-kb upstream and 3-kb downstream)

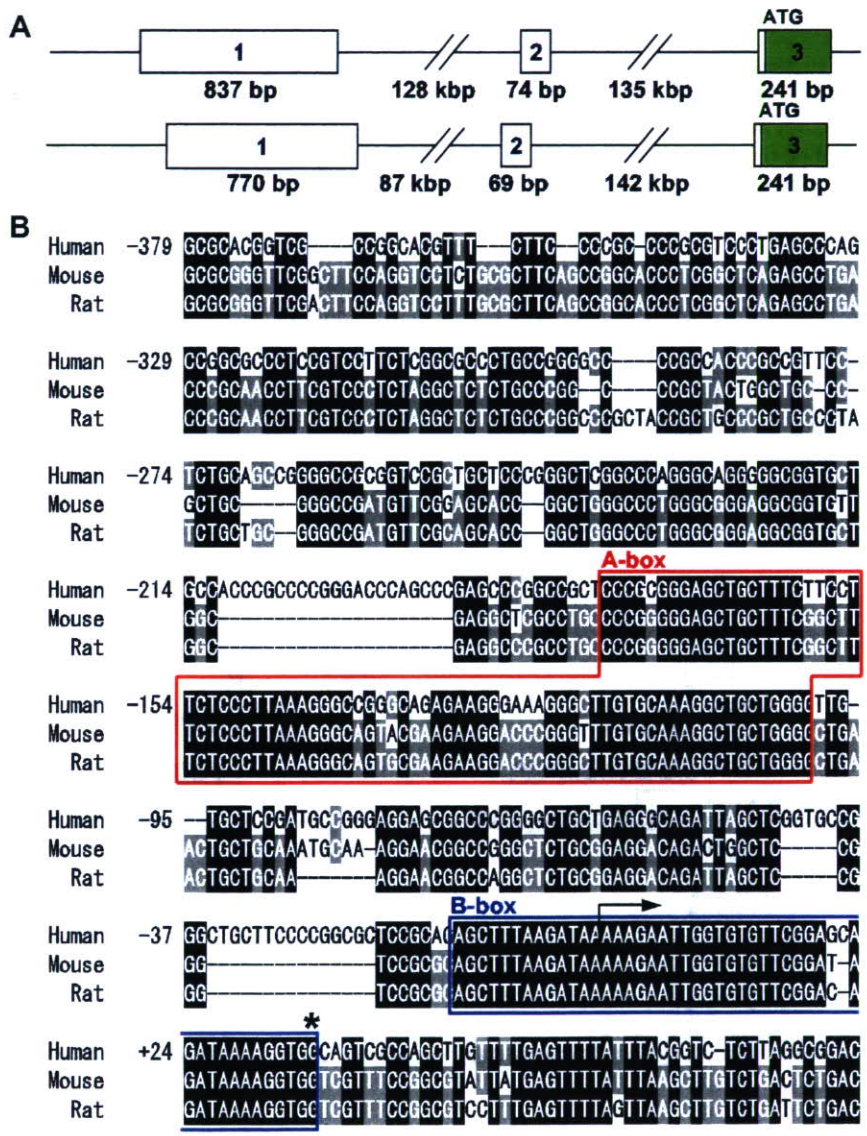

Fig. 1. Identification of the human and mouse Sox6 promoters. (A) The schematic structure of the human and mouse Sox6 genes transcribed in embryos. Exons are denoted by open boxes. Coding regions are shaded. (B) Comparison of the proximal promoter sequences of the human, mouse, and rat Sox6 genes. Conserved nucleotides in all three species are denoted by white letters shaded in black. Conserved nucleotides in two species were denoted by white letters shaded in gray. Two highly conserved regions are boxed. The A-box is boxed by a blue line, and the B-box by a red line. The positions of the nucleotides in the human SOX6 gene are demonstrated on the left side of the sequences. The position of the putative transcription start site in the human gene is denoted by an arrow; that in the mouse gene by an asterisk. (For interpretation of the references to color in this figure legend, the reader is referred to the web version of this paper.)

as a query sequence. The search revealed that the entire genomic sequence in the region was relatively poorly conserved with only two short highly conserved regions among the rats, mice, and humans. These two highly conserved sequences were both located near the transcription start region, and we called them A-box (79 bp) and B-box (48 bp), respectively (Fig. 1B). The A-box was 85% (67/79) conserved among the three species and the B-box, 96% (46/48). To evaluate the *in vivo* activity of the identified embryonic Sox6 promoter during the sequential differentiation stages of the chondrocytes in the developing limb, we designed an anti-sense RNA probe for the mouse exon 1, which was specifically transcribed by this promoter, and performed *in situ* hybridization using the mouse E17.5 growth plate (Supplementary Fig. 1). The Sox6 exon 1 transcript was widely expressed in the chondrocytes of the resting, proliferative and prehypertrophic zones, similar to those of the Sox6 mRNA and Sox9 mRNA detected by the anti-sense RNA probes for the coding regions.

Identification of the core enhancer of the human Sox6 promoter (CES6)

To determine the regulatory element of the human SOX6 gene expression, luciferase-reporters containing a short (517 bp) or a long (2089 bp) promoter fragment with exon 1 as well as luciferase-reporters containing tandem repeats of the A-box and the B-box were constructed (Fig. 2). ATDC5 cells [19], which differentiate into chondrocytes upon treatment with insulin and express Sox6 mRNA (Ikeda et al., unpublished data), and the human liver-derived HuH-7 cells, which express moderate levels of endogenous SOX6 mRNA [15], were used as the host cells. The luciferase-reporter plasmids were transfected into these cells, and the promoter activities were examined. Both the short and the long promoters of the human SOX6 did not show any apparent transcriptional activity. On the other hand, the 79-bp A-box exhibited a strong transcriptional activity in proportion to the repeat number. The activity of the A-box was upregulated by the overexpression of SOX9. On the other hand, the tandem repeats of the B-box did not show any apparent transcriptional activity in the presence or absence of the SOX9 overexpression. To evaluate the activity of the A-box in differentiating chondrocytes, we stably transfected the ATDC5 cells with the 4xA-box-DsRed2 (red fluorescent protein) reporter plasmid and found that these cells showed a fluorescence only upon chondrogenic differentiation stimulated by insulin [19] (Supplementary Fig. 2). These results suggest that the A-box sequence is transactivated in response to the chondrogenic differentiation.

To further narrow down the regulatory element, we compared the luciferase activities of the 5′ half (A1) and the 3′ half (A2) of the A box in both cell lines. The activity of the A-box was dependent on the 3′ half both at the basal level and in response to the Sox9 overexpression (Fig. 3A). The A2 contained two regions resembling the high mobility group (HMG) binding motifs. They were slightly different from the known SOX9-binding sequences identified in the type II collagen and type XI collagen genes [20,21], and the mutations in the HMG binding motifs did not affect the basal activity

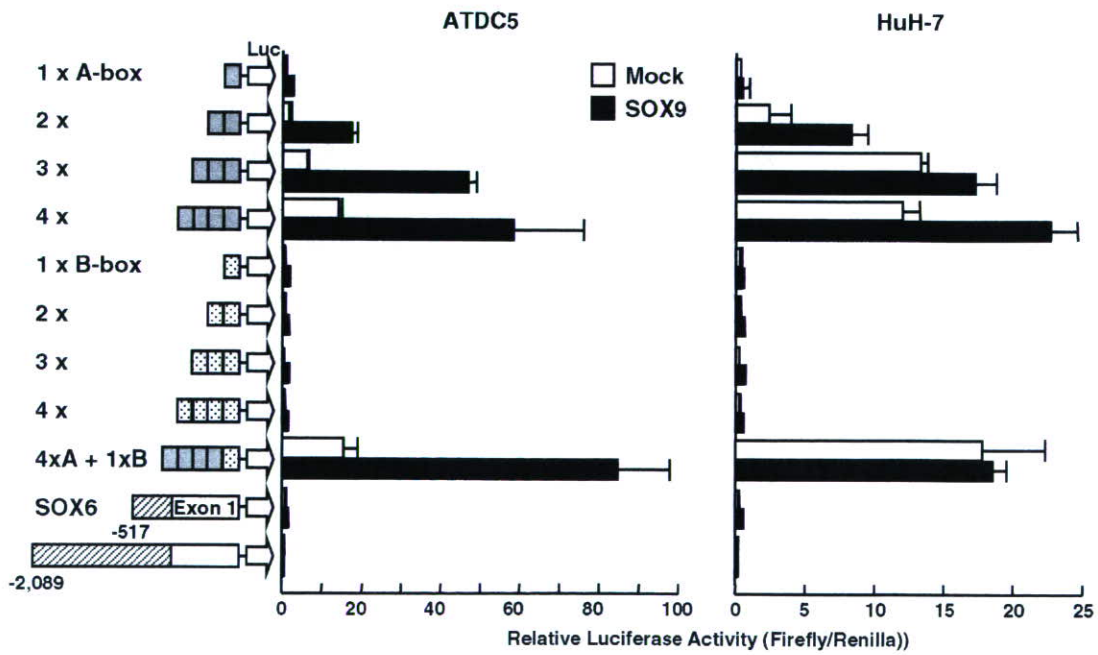

Fig. 2. Functional characterization of the human embryonic SOX6 promoter. Results of the luciferase-reporter assays. Basic activities of the single and multi-copies of the A-box or B-box and those of the long (−2089) and short (−517) embryonic SOX6 promoter are denoted by white bars; responses to SOX9 overexpression are denoted by black bars. Mock, transfection with the empty vector. Each bar denotes an average ± SD.

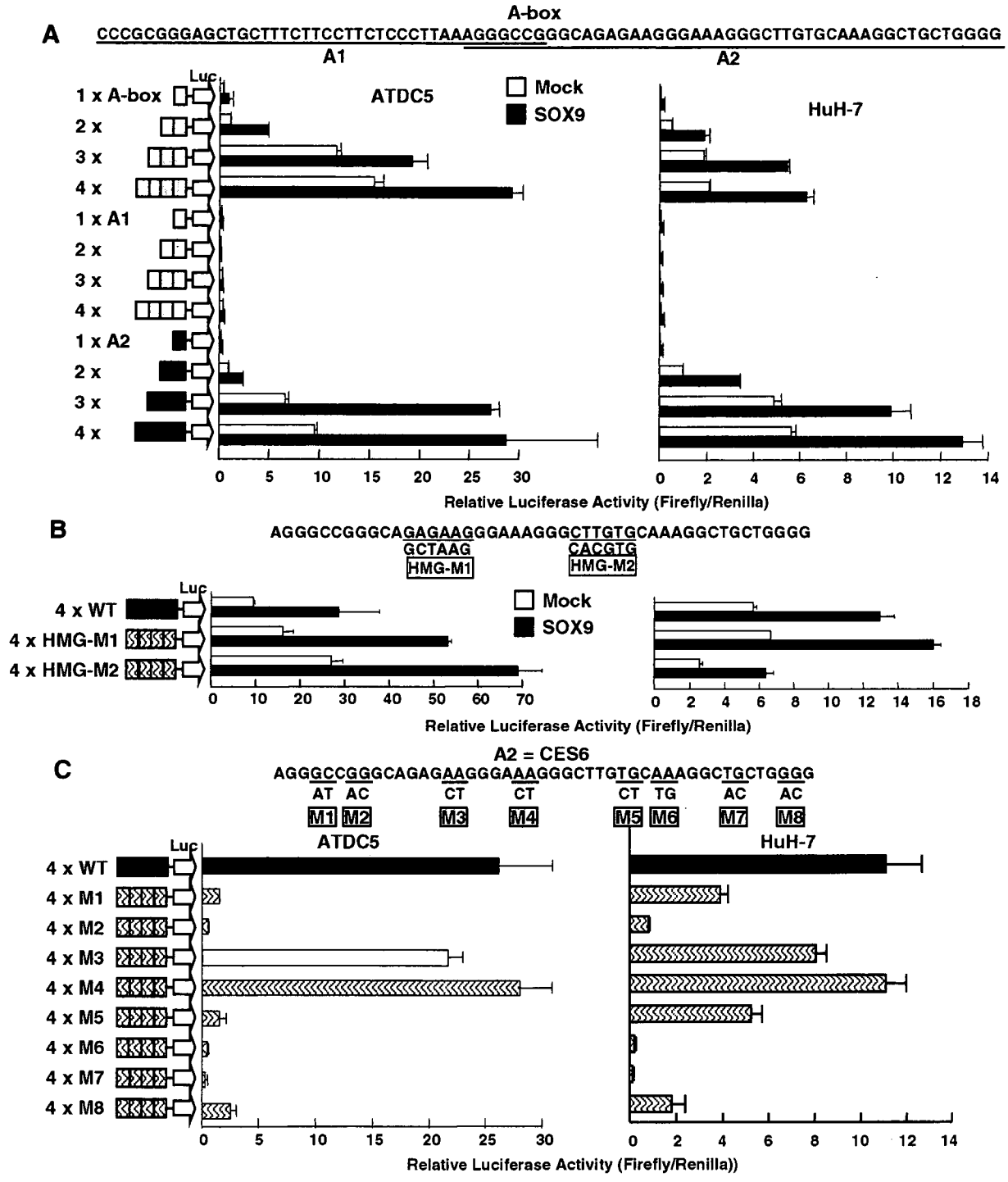

Fig. 3. Functional characterization of A-box and identification of the core enhancer of SOX6 (CES6). (A) The A-box was divided into two overlapping fragments, A1 and A2, and the transcriptional activities of the single or multi-copies of each fragment were estimated by luciferase-reporter assays. White bars indicate the basal activities, and black bars indicate the activities in response to the SOX9 overexpression. Mock, transfection with the empty vector. (B) Two HMG-like motifs underlined in the A2 fragment were mutated as indicated below, and four copies of them were inserted into pGL3. The activities of the wild-type and mutant constructs were evaluated with or without co-transfection of SOX9. Mock, transfection with the empty vector. (C) Eight different sites in the A2 fragment were randomly mutated as indicated and the basal activities of 4 copies of the wild-type or mutant fragments were estimated by luciferase-reporter assays.

or the response to the SOX9 overexpression of the A2 sequence (Fig. 3B). In addition, we failed to show the direct binding of the *in vitro* translated SOX9 protein to the A2 sequence (data not shown), suggesting indirect activation of the A2 by SOX9. On the other hand, when we randomly introduced the 2-bp mutations at eight posi-

tions in the A2 sequence, the two 3′ and four 5′ mutations attenuated the transcriptional activity (Fig. 3C), indicating that the entire A2 region is the minimum core enhancer of the SOX6 transcription (CES6) with a high sequence specificity. The electrophoretic mobility shift assay using nuclear extracts derived from the HuH-7 cells revealed that there was a nuclear factor(s) that could bind to the CES6 (Supplementary Fig. 3). Competition assays using various cold mutant probes revealed that the M6 mutant failed to fully compete, suggesting that the core transcription factor(s) regulating the CES6-binding protein complex might bind the wild-type sequence containing the M6 area. We speculate that SOX9 acts on CES6 by interacting with other CES6 binding transcription factor(s) rather than directly binding to the DNA.

CCAAT enhancer binding protein (C/EBP) as a CES6 binding factor

We then attempted to identify the CES6 binding transcription factor(s). Since a database search using the TFSEARCH website identified a C/EBP binding motif [22] within CES6, we examined whether the C/EBPs could transactivate the wild-type 517-bp promoter plus exon 1 construct as well as the 4xCES6 construct. The wild-type SOX6 promoter activity was elevated by the overexpression of C/EBPα, and more strongly by that of C/EBPβ, in both the ATDC5 and HuH-7 cells, while the overexpression of C/EBP did not upregulate the activity of the 4xCES6 construct (Fig. 4A and data not shown). We then created the 4xCES6 mutant constructs that lacked the predicted C/

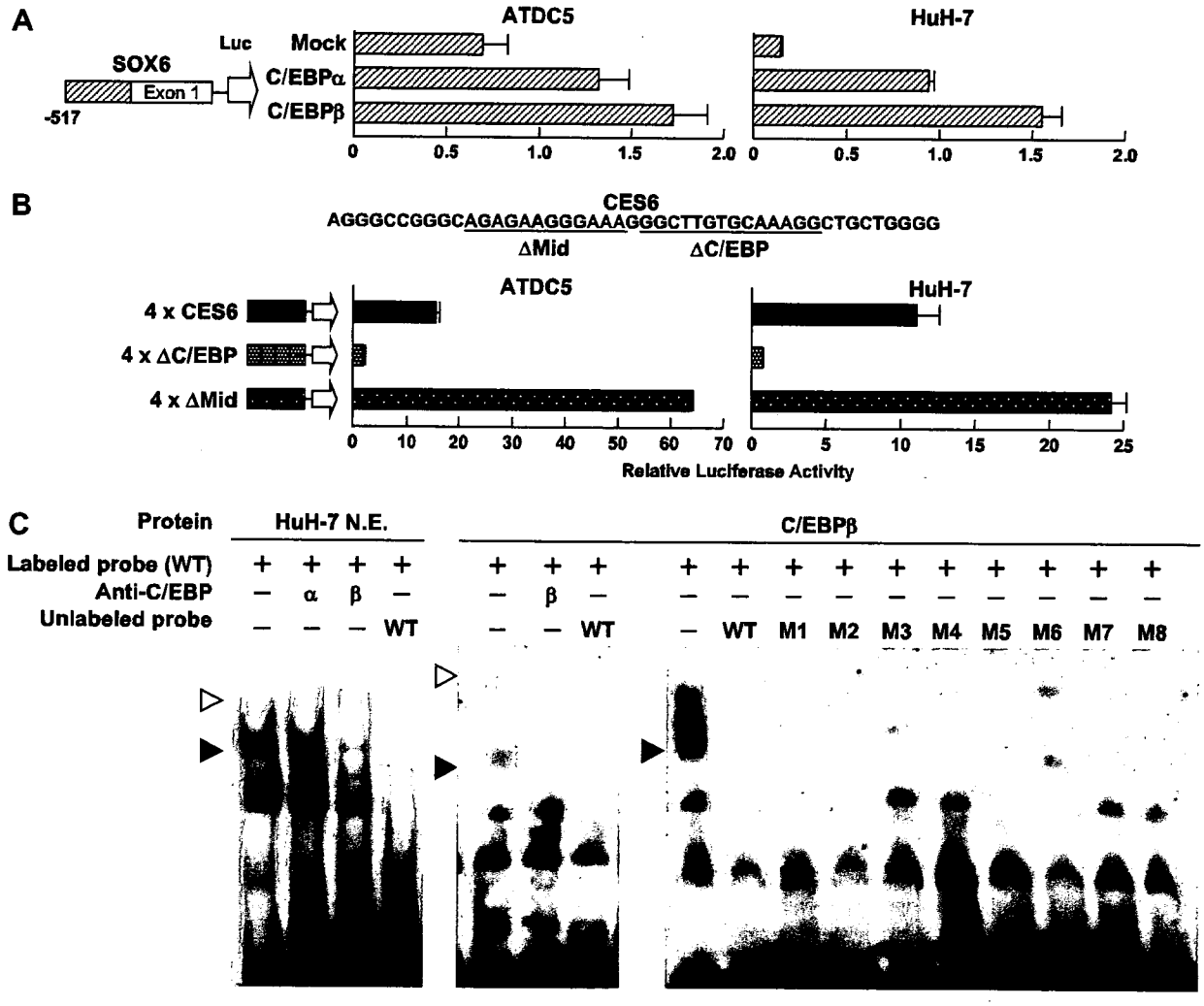

Fig. 4. Interactions of C/EBPβ with the embryonic SOX6 promoter. (A) Luciferase-reporter analysis of the short (−517) promoter of SOX6 upon co-transfection with C/EBPα or C/EBPβ. Mock, co-transfection with the empty vector (Clontech). (B) Luciferase-reporter analysis of a deletion mutant of CES6 lacking the predicted C/EBP binding motif (underlined, ΔCEBP) and a deletion mutant of CES6 lacking the unrelated area (underlined, ΔMid). (C) The electrophoretic mobility shift assays of CES6 and C/EBP. HuH-7 N.E., nuclear extracts of HuH-7; C/EBPβ, *in vitro* translated C/EBPβ. WT, wild-type CES6 probe. M1–M8, mutant CES6 probes. The DNA–protein complex containing C/EBPβ is indicated by black arrowheads, and the super-shift complex is indicated by white arrowheads.

EBP binding motif (ΔC/EBP) or the mid-region that did not contain the C/EBP motif (ΔMid), and compared them with the wild-type 4xCES6. In contrast to the comparable or higher activity of the 4xΔMid construct to the wild-type, the 4xΔC/EBP almost completely lost its activity (Fig. 4B), suggesting the crucial role of the C/EBP family in the transactivation of the CES6. Immunoblot analysis revealed that both C/EBPα and β were endogenously expressed in the nucleus of HuH-7 cells (Supplementary Fig. 4). The electrophoretic mobility shift assay revealed that the protein–CES6 complex was partially supershifted by the addition of the anti-C/EBPβ antibody, but not by the anti-C/EBPα antibody (Fig. 4C, left panel). When we used the C/EBPβ protein prepared by *in vitro* translation, it became bound to CES6, with the complex being competed by excessive unlabeled probes and being supershifted by the anti-C/EBPβ antibody (Fig. 4C, middle panel). When the competition by the mutant probes was examined, M6 and M7 did not fully compete the binding of C/EBPβ to the wild-type probe. These data suggest that the wild-type sequence containing the M6 and M7 areas is important for the binding of C/EBPβ to CES6. Mutations in CES6 that were dispensable for the C/EBPβ binding attenuated the transcriptional activity of CES6 (M1, M2 and M5, M8). The sequence specificity of the CES6-binding of the HuH-7 nuclear extracts was slightly different from that of the *in vitro* translated C/EBPβ protein. These results suggest the presence of other transcription factor(s) that cooperatively work with C/EBPβ to maintain the activity of CES6. Because we could not find any binding motifs for the known transcription factors, the CES6-binding transcription factor(s) that interact with C/EBPβ and transactivate the SOX6 gene may be a novel one.

In conclusion, we identified the embryonic SOX6 promoter and its core enhancer CES6. The identified promoter was transactivated by SOX9 and C/EBPβ. C/EBPβ directly bound to CES6, while SOX9 did not. This unique property of the identified SOX6 promoter will provide a useful clue to identifying a network of transcription factors for chondrogenic differentiation. We also believe that comparative genomics can be a useful and potent tool for analyzing the cis-acting regulatory elements for other genes that control chondrogenesis.

Acknowledgments

This study was supported by Grants-in-Aid for Scientific Research from the Japanese Ministry of Education, Culture, Sports, Science and Technology (#16390430, #17591549, and #18209047).

Appendix A. Supplementary data

Supplementary data associated with this article can be found, in the online version, at doi:10.1016/j.bbrc.2007.03.133.

References

[1] J.A. Buckwalter, H.J. Mankin, A.J. Grodzinsky, Articular cartilage and osteoarthritis, Instr. Course Lect. 54 (2005) 465–480.
[2] B. de Crombrugghe, V. Lefebvre, R.R. Behringer, W. Bi, S. Murakami, W. Huang, Transcriptional mechanisms of chondrocyte differentiation, Matrix Biol. 19 (2000) 389–394.
[3] M. Sen, Y.H. Cheng, M.B. Goldring, M.K. Lotz, D.A. Carson, WISP3-dependent regulation of type II collagen and aggrecan production in chondrocytes, Arthritis Rheum. 50 (2004) 488–497.
[4] V. Lefebvre, P. Li, B. de Crombrugghe, A new long form of Sox5 (L-Sox5), Sox6 and Sox9 are coexpressed in chondrogenesis and cooperatively activate the type II collagen gene, EMBO J. 17 (1998) 5718–5733.
[5] H. Akiyama, M.C. Chaboissier, J.F. Martin, A. Schedl, B. de Crombrugghe, The transcription factor Sox9 has essential roles in successive steps of the chondrocyte differentiation pathway and is required for expression of Sox5 and Sox6, Genes Dev. 16 (2002) 2813–2828.
[6] W. Bi, J.M. Deng, Z. Zhang, R.R. Behringer, B. de Crombrugghe, Sox9 is required for cartilage formation, Nat. Genet. 22 (1999) 85–89.
[7] T. Wagner, J. Wirth, J. Meyer, B. Zabel, M. Held, J. Zimmer, J. Pasantes, F.D. Bricarelli, J. Keutel, E. Hustert, U. Wolf, N. Tommerup, W. Schempp, G. Scherer, Autosomal sex reversal and campomelic dysplasia are caused by mutations in and around the SRY-related gene SOX9, Cell 79 (1994) 1111–1120.
[8] S. McDowall, A. Argentaro, S. Ranganathan, P. Weller, S. Mertin, S. Mansour, J. Tolmie, V. Harley, Functional and structural studies of wild type SOX9 and mutations causing campomelic dysplasia, J. Biol. Chem. 274 (1999) 24023–24030.
[9] W. Bi, W. Huang, D.J. Whitworth, J.M. Deng, Z. Zhang, R.R. Behringer, B. de Crombrugghe, Haploinsufficiency of Sox9 results in defective cartilage primordia and premature skeletal mineralization, Proc. Natl. Acad. Sci. USA 98 (2001) 6698–6703.
[10] J. Giordano, H.M. Prior, J.S. Bamforth, M.A. Walter, Genetic study of SOX9 in a case of campomelic dysplasia, Am. J. Med. Genet. 98 (2001) 176–181.
[11] J.W. Foster, M.A. Dominguez-Steglich, S. Guioli, G. Kowk, P.A. Weller, M. Weissenbach, S. Mansour, I.D. Young, P.N. Goodfellow, J.D. Brook, A.J. Shafer, Campomelic dysplasia and autosomal sex reversal caused by mutations in an SRY-related gene, Nature 372 (1994) 525–530.
[12] H. Akiyama, M.C. Chaboissier, R.R. Behringer, D.H. Rowitch, A. Schedl, J.A. Epstein, B. de Crombrugghe, Essential role of Sox9 in the pathway that controls formation of cardiac valves and septa, Proc. Natl. Acad. Sci. USA 101 (2004) 6502–6507.
[13] Q. Zhao, H. Eberspaecher, V. Lefebvre, B. de Crombrugghe, Parallel expression of Sox9 and Col2a1 in cells undergoing chondrogenesis, Dev. Dyn. 209 (1997) 377–386.
[14] P. Smits, P. Li, J. Mandel, Z. Zhang, J.M. Deng, R.R. Behringer, B. de Crombrugghe, V. Lefebvre, The transcription factors L-Sox5 and Sox6 are essential for cartilage formation, Dev. Cell 1 (2001) 277–290.
[15] T. Ikeda, S. Kamekura, A. Mabuchi, I. Kou, S. Seki, T. Takato, K. Nakamura, H. Kawaguchi, S. Ikegawa, U.I. Chung, The combination of SOX5, SOX6, and SOX9 (the SOX trio) provides signals sufficient for induction of permanent cartilage, Arthritis Rheum. 50 (2004) 3561–3573.
[16] R. Fernandez-Lloris, F. Vinals, T. Lopez-Rovira, V. Harley, R. Bartrons, J.L. Rosa, F. Ventura, Induction of the Sry-related factor SOX6 contributes to bone morphogenetic protein-2-induced chondroblastic differentiation of C3H10T1/2 cells, Mol. Endocrinol. 17 (2003) 1332–1343.
[17] S.F. Altschul, T.L. Madden, A.A. Schaffer, J. Zhang, Z. Zhang, W. Miller, D.J. Lipman, Gapped BLAST and PSI-BLAST: a new generation of protein database search programs, Nucleic Acids Res. 25 (1997) 3389–3402.

[18] O. Cohen-Barak, N. Hagiwara, M.F. Arlt, J.P. Horton, M.H. Brilliant, Cloning, characterization and chromosome mapping of the human SOX6 gene, Gene 265 (2001) 157–164.

[19] C. Shukunami, C. Shigeno, T. Atsumi, K. Ishizeki, F. Suzuki, Y. Hiraki, Chondrogenic differentiation of clonal mouse embryonic cell line ATDC5 in vitro: differentiation-dependent gene expression of parathyroid hormone (PTH)/PTH-related peptide receptor, J. Cell Biol. 133 (1996) 457–468.

[20] L.C. Bridgewater, V. Lefebvre, B. de Crombrugghe, Chondrocyte-specific enhancer elements in the Col11a2 gene resemble the Col2a1 tissue-specific enhancer, J. Biol. Chem. 273 (1998) 14998–15006.

[21] G. Zhou, V. Lefebvre, Z. Zhang, H. Eberspaecher, B. de Crombrugghe, Three high mobility group-like sequences within a 48-base pair enhancer of the Col2a1 gene are required for cartilage-specific expression in vivo, J. Biol. Chem. 273 (1998) 14989–14997.

[22] S. Akira, H. Isshiki, T. Sugita, O. Tanabe, S. Kinoshita, Y. Nishio, T. Nakajima, T. Hirano, T. Kishimoto, A nuclear factor for IL-6 expression (NF-IL6) is a member of a C/EBP family, EMBO J. 9 (1990) 1897–1906.

DEVELOPMENTAL DYNAMICS 236:1876–1890, 2007

RESEARCH ARTICLE

Runx2 Determines Bone Maturity and Turnover Rate in Postnatal Bone Development and Is Involved in Bone Loss in Estrogen Deficiency

Zenjiro Maruyama,[1,5†] Carolina A. Yoshida,[1†] Tatsuya Furuichi,[1†‡] Norio Amizuka,[2] Masako Ito,[8] Ryo Fukuyama,[3] Toshihiro Miyazaki,[1] Hideki Kitaura,[6] Kouhei Nakamura,[1,7] Takashi Fujita,[1] Naoko Kanatani,[1] Takeshi Moriishi,[1] Kei Yamana,[4] Wenguang Liu,[1] Hiroshi Kawaguchi,[5] Kozo Nakamura,[5] and Toshihisa Komori[1*]

Runx2 is an essential transcription factor for osteoblast differentiation. However, the functions of Runx2 in postnatal bone development remain to be clarified. Introduction of dominant-negative (dn)-*Runx2* did not inhibit *Col1a1* and *osteocalcin* expression in mature osteoblastic cells. In transgenic mice that expressed dn-*Runx2* in osteoblasts, the trabecular bone had increased mineralization, increased volume, and features of compact bone, and the expression of major bone matrix protein genes was relatively maintained. After ovariectomy, neither osteolysis nor bone formation was enhanced and bone was relatively conserved. In wild-type mice, Runx2 was strongly expressed in immature osteoblasts but downregulated during osteoblast maturation. These findings indicate that the maturity and turnover rate of bone are determined by the level of functional Runx2 and Runx2 is responsible for bone loss in estrogen deficiency, but that Runx2 is not essential for maintenance of the expression of major bone matrix protein genes in postnatal bone development and maintenance. *Developmental Dynamics 236:1876–1890, 2007.* © 2007 Wiley-Liss, Inc.

Key words: Runx2; bone; osteoblast; osteocyte; osteoclast; bone metabolism

Accepted 10 April 2007

INTRODUCTION

Bone is composed of compact bone and cancellous bone. In long bones, the shaft (cortical bone) consists of compact bone, and the inside of the shaft (trabecular bone), which is a three-dimensional lattice of branching bony spicules, consists of cancellous bone. Compact bone is mature bone, because it is composed of densely packed, highly organized collagen fibrils with high mineralization, and is relatively resistant to osteolysis. In contrast, cancellous bone is less mature, because it is composed of loosely

[1]Department of Cell Biology, Unit of Basic Medical Sciences, Nagasaki University Graduate School of Biomedical Sciences, Nagasaki, Japan
[2]Center for Transdisciplinary Research, Niigata University, Niigata, Japan
[3]Laboratory of Pharmacology, Faculty of Pharmaceutical Sciences, Hiroshima International University, Kure, Japan
[4]Teijin Institute for Biomedical Research, Teijin Ltd., Tokyo, Japan
[5]Department of Orthopaedic Surgery, The University of Tokyo, Tokyo, Japan
[6]Division of Orthodontic and Biomedical Engineering, Nagasaki University Graduate School of Biomedical Sciences, Nagasaki, Japan
[7]Department of Periodontology, Unit of Translational Medicine, Nagasaki University Graduate School of Biomedical Sciences, Nagasaki, Japan
[8]Department of Radiology and Radiation Biology, Nagasaki University Graduate School of Biomedical Sciences, Nagasaki, Japan
Grant sponsor: Ministry of Education, Culture, Sports, Science, and Technology, Japan; Grant sponsor: Sumitomo Foundation.
†Zenjiro Maruyama, Carolina A. Yoshida, and Tatsuya Furuichi contributed equally to this work.
‡Tatsuya Furuichi's present address is Laboratory for Bone and Joint Diseases, SNP Research Center, The Institute of Physical and Chemical Research (RIKEN), Tokyo 108-8639, Japan.
***Correspondence to: Toshihisa Komori, Department of Cell Biology, Unit of Basic Medical Sciences, Nagasaki University Graduate School of Biomedical Sciences, 1-7-1 Sakamoto, Nagasaki 852-8588, Japan. E-mail: komorit@nagasaki-u.ac.jp**

DOI 10.1002/dvdy.21187
Published online 11 May 2007 in Wiley InterScience (www.interscience.wiley.com).

organized collagen fibrils with low mineralization, and it is easily resorbed and plays an important role in calcium homeostasis (Marks and Odgren, 2002).

Runt-related transcription factor 2 (Runx2) is a transcription factor that belongs to the Runx family and is involved in many aspects of skeletal development (Komori, 2005). Upon forming a heterodimer with core binding factor β (Cbfβ), Runx2 acquires DNA-binding activity and regulates transcriptional activity (Kundu et al., 2002; Miller et al., 2002; Yoshida et al., 2002; Kanatani et al., 2006). There are two Runx2 isoforms, type I Runx2 and type II Runx2, which have different N-termini, and type I Runx2 is more dependent on Cbfb than type II Runx2 for their functional activities (Kanatani et al., 2006). *Runx2*-deficient mice lack osteoblasts and show a complete lack of bone formation, demonstrating that Runx2 is essential for osteoblast differentiation (Komori et al., 1997; Otto et al., 1997). Runx2 also plays important roles in chondrocyte maturation, maintenance of the chondrocyte phenotype, and vascular invasion into cartilage (Komori, 2005; Zelzer et al., 2001). Furthermore, Runx2 regulates *RANKL* and *OPG* expression stimulating osteoclast differentiation (Enomoto et al., 2003). These findings indicate that Runx2 functions as a key molecule in skeletal development.

The DNA-binding sites of Runx2 in major bone matrix protein genes including the *Col1a1, osteopontin, bone sialoprotein,* and *osteocalcin* genes, have been identified, and Runx2 induced the expression of these genes or activated their promoters (Ducy et al., 1997, 1999; Sato et al., 1998; Harada et al., 1999; Javed et al., 1999; Kern et al., 2001). Furthermore, the expression of dominant-negative (dn)-*Runx2* under the control of osteocalcin promoter completely abrogated the expression of major bone matrix protein genes in postnatal bone development (Ducy et al., 1999). These findings indicate that Runx2 plays an important role in the expression of major bone matrix protein genes. In transgenic mice that express *Runx2* under the control of the *Col1a1* promoter, however, the cortical bone was composed of woven bone due to the inhibition of osteoblast differentiation at the late stage, which was shown by the reductions in the mRNA expression of *alkaline phosphatase (ALP), Col1a1, osteocalcin,* and *matrix metalloproteinase 13 (MMP13),* all of which are normally upregulated according to the degree of osteoblast differentiation (Liu et al., 2001; Geoffroy et al., 2002). Therefore, the function of Runx2 in postnatal bone development is controversial.

To clarify the function of Runx2 in osteoblasts, we inhibited the function of Runx2 using dn-*Runx2* in in vitro and in vivo studies. We show here that the maturity and turnover rate of bone are determined by the level of functional Runx2, and that Runx2 is involved in bone loss in estrogen deficiency. However, Runx2 was not essential for maintenance of major bone matrix protein gene expression in postnatal bone development and maintenance.

RESULTS

Dn-Runx2 Inhibited ALP Activity in Osteoblast Precursors But Did Not Suppress Bone Matrix Protein Gene Expression in Mature Osteoblastic Cells in Vitro

Using two cDNAs, one containing the *runt* domain with the N-terminus of type I *Runx2* (long form) and the other containing only the *runt* domain (short form) (Fig. 1A), we examined their dominant-negative (dn) activity against Runx2. Both forms had no capacity for transcriptional activation in luciferase assays using oligonucleotides containing 6 repeats of the consensus Runx2 binding sequence, but both inhibited Runx2-dependent transcription dose-dependently (Fig. 1B and C). First, we examined their dominant-negative effects on ALP activity, which is an early marker of osteoblast differentiation, using primary calvarial cells as osteoblastic precursors and an immature mesenchymal cell line, C2C12, which differentiates into osteoblasts in the presence of rhBMP-2 (Fig. 1D and E). Adenoviral introduction of *Runx2* upregulated ALP expression in primary calvarial cells and in rhBMP-2-treated C2C12 cells, whereas adenoviral introduction of either form of dn-*Runx2* downregulated ALP expression in comparison with the level of ALP expression in enhanced green fluorescence protein (EGFP)-expressing vector-infected cells. These findings indicate that Runx2 induces an early marker of osteoblast differentiation, while dn-Runx2 inhibits it, and that the two forms of dn-*Runx2* have similar efficiencies in vitro. We previously observed that transgenic mice overexpressing either form of dn-*Runx2* under the control of the *Col2a1* promoter exhibited inhibition of chondrocyte maturation, although the strong dominant-negative effect was observed more frequently among transgenic mice expressing the long form of dn-*Runx2* (Ueta et al., 2001, unpublished observation).

We next examined the effect of adenoviral introduction of dn-*Runx2* on endogenous *Col1a1* and *osteocalcin* expression in vitro. As mature osteoblasts express high levels of *Col1a1* and *osteocalcin* in vivo, we analyzed their expression in mature osteoblastic cells. Primary calvarial cells and the immature osteoblastic cell line MC3T3-E1 were cultured for 10 days after confluence to generate mature osteoblastic cells. We also used the mature osteoblastic cell line MLO-A5. In primary calvarial cells, MC3T3-E1 cells, and MLO-A5 cells, adenoviral introduction of *Runx2* upregulated *osteocalcin* expression but had no effect on *Col1a1* expression in comparison with the respective level in EGFP-expressing cells, while adenoviral introduction of dn-*Runx2* had no effect on *Col1a1* nor *osteocalcin* expression (Fig. 1F–H). These findings indicate that exogenously introduced *Runx2* upregulates *osteocalcin* expression in mature osteoblastic cells, but that Runx2 is not absolutely required for the steady-state expression of *Col1a1* and *osteocalcin* in mature osteoblastic cells in vitro.

Generation of dn-*Runx2* Transgenic Mice

We generated transgenic mice that express dn-*Runx2* under the control of the 2.3-kb promoter of mouse *Col1a1* (Fig. 2A). We previously reported that the promoter directs transgene ex-

pression to immature and mature osteoblasts (Liu et al., 2001). Two lines of dn-*Runx2* transgenic mice were established from two F_0 mice, and they highly expressed the long form of dn-*Runx2*. The two established lines of transgenic mice showed significant levels of transgene expression, as confirmed by Northern blot and Western blot analyses (Fig. 2B and C). The two lines of transgenic mice showed similar phenotypes, and detailed data on transgenic mouse line 1 are reported. In transgenic mouse line 1, the transgene expression was much stronger than endogenous *Runx2* expression (Fig. 2D). To confirm that the protein encoded by the transgene had a dominant-negative effect on Runx2 function in vivo, dn-*Runx2* transgenic mice were mated with transgenic mice that expressed *Runx2* under the control of the same *Col1a1* promoter, which were described previously (Liu et al., 2001). The *Runx2* transgenic mice showed osteopenia with fractures, reduced *osteocalcin* expression, and a reduced number of osteocytes (Liu et al., 2001) (Fig. 2E–H). However, the double transgenic mice, which expressed both the *Runx2* and dn-*Runx2* transgenes, showed no fractures and had a normal level of *osteocalcin* expression and normal osteocyte number, although the mice were mildly osteopenic (Figs. 2E–H). The mild os-

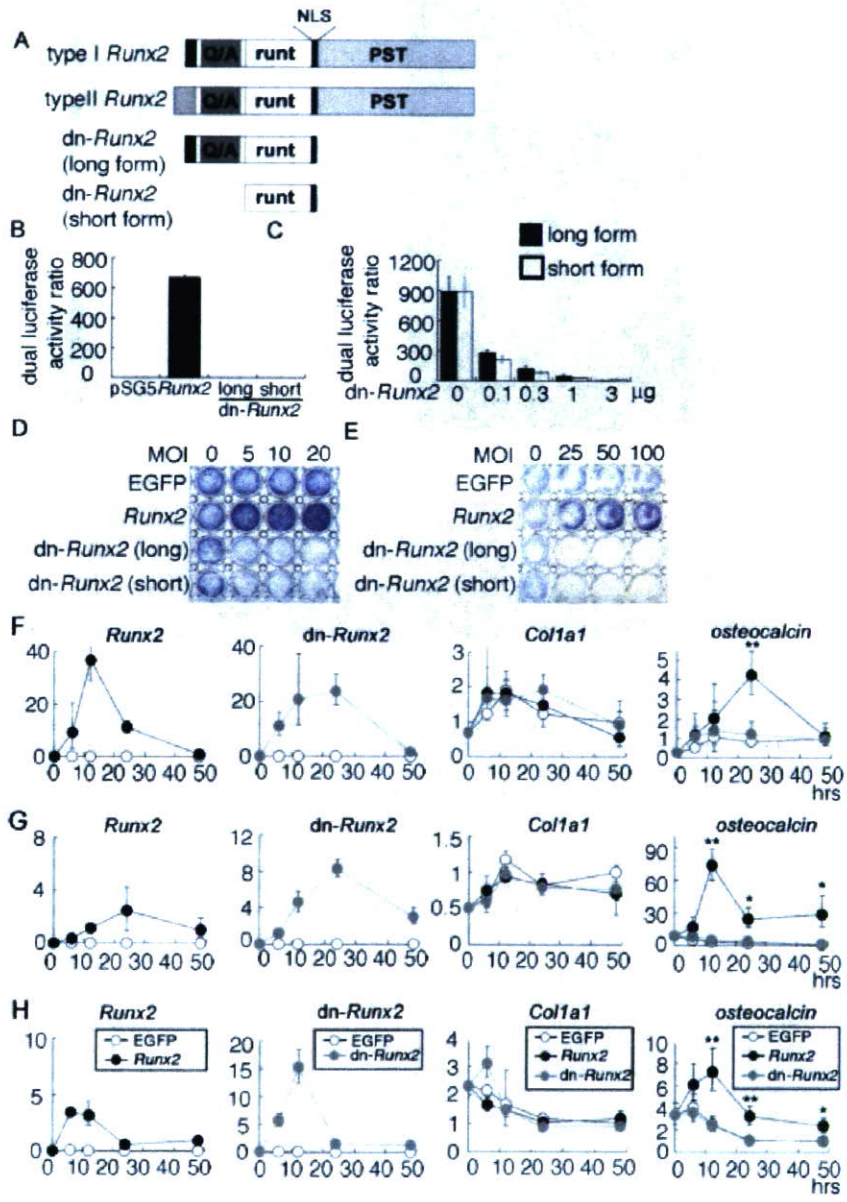

Fig. 1.

Fig. 1. In vitro studies. **A:** Diagrams of the two Runx2 isoforms with different N-termini and two dominant-negative forms of Runx2. The type I and type II Runx2 isoforms have different N-termini (Harada et al., 1999). Q/A, glutamine and alanine stretch; runt, runt homology region; NLS, nuclear localization sequence; PST, proline-, serine-, and threonine-rich region. **B:** Transcriptional activation by *Runx2*- and dn-*Runx2*-expressing vectors. The reporter plasmid containing 6xOSE2 was cotransfected with empty pSG5 vector, type II *Runx2*-expressing vector, dn-*Runx2* (long)-expressing vector, or dn-*Runx2* (short)-expressing vector into C3H10T1/2 cells. Data are presented as mean ± S.D. of 3 wells. **C:** Inhibition of Runx2-dependent transcription by dominant-negative forms of Runx2. Reporter assays were carried out using stable C3H10T1/2 transfectants of type II *Runx2*. The reporter plasmid containing 6 × OSE2 was cotransfected with increasing amounts of dn-*Runx2* (long)-expressing or dn-*Runx2* (short)-expressing vector. Data are presented as mean ± S.D. of 3 wells. **D,E:** Inhibition of ALP activity by dn-*Runx2*. Primary cultured calvarial cells at 70% confluency (D) and C2C12 cells at confluency (E) were infected with EGFP-expressing, type II *Runx2*-expressing, dn-*Runx2* (long)-expressing, or dn-*Runx2* (short)-expressing adenovirus at the indicated multiplicity of infection (MOI). One day after infection, the infected C2C12 cells were stimulated with rhBMP-2 (100 ng/ml) for 6 days and stained for ALP. **F–H:** Effect of adenoviral introduction of *Runx2* or dn-*Runx2* on *Col1a1* and *osteocalcin* expression. Primary cultured calvarial cells (F) and MC3T3-E1 cells (G), which had been cultured for 10 days after confluency, and MLO-A5 cells (H) at confluency were infected with EGFP-expressing, type II *Runx2*-expressing, or dn-*Runx2* (short)-expressing adenovirus at a MOI of 10 in primary cultured calvarial cells and MC3T3-E1 cells and a MOI of 5 in MLO-A5 cells. RNA was extracted from the infected cells at the indicated times after infection. The time courses of the expression of the transgene, *Col1a1*, and *osteocalcin* were monitored by real-time RT-PCR. The level of *Runx2* mRNA expression in cells infected with type II *Runx2*-expressing adenovirus at 48 hr and the level of dn-*Runx2* mRNA expression in cells infected with dn-*Runx2*-expressing adenovirus at 48 hr were defined as 1, and the relative levels of *Runx2* and dn-*Runx2* mRNA expression are shown. The levels of *Col1a1* and *osteocalcin* mRNA expression in cells infected with EGFP-expressing adenovirus at 48 hr were defined as 1, and relative levels are shown. Data are presented as mean ± S.D. of 3 wells. In F–H, $^{*}P < 0.05$ and $^{**}P < 0.01$ vs. EGFP-expressing cells. In B–H, similar results were obtained in three or four independent experiments and representative data are shown.

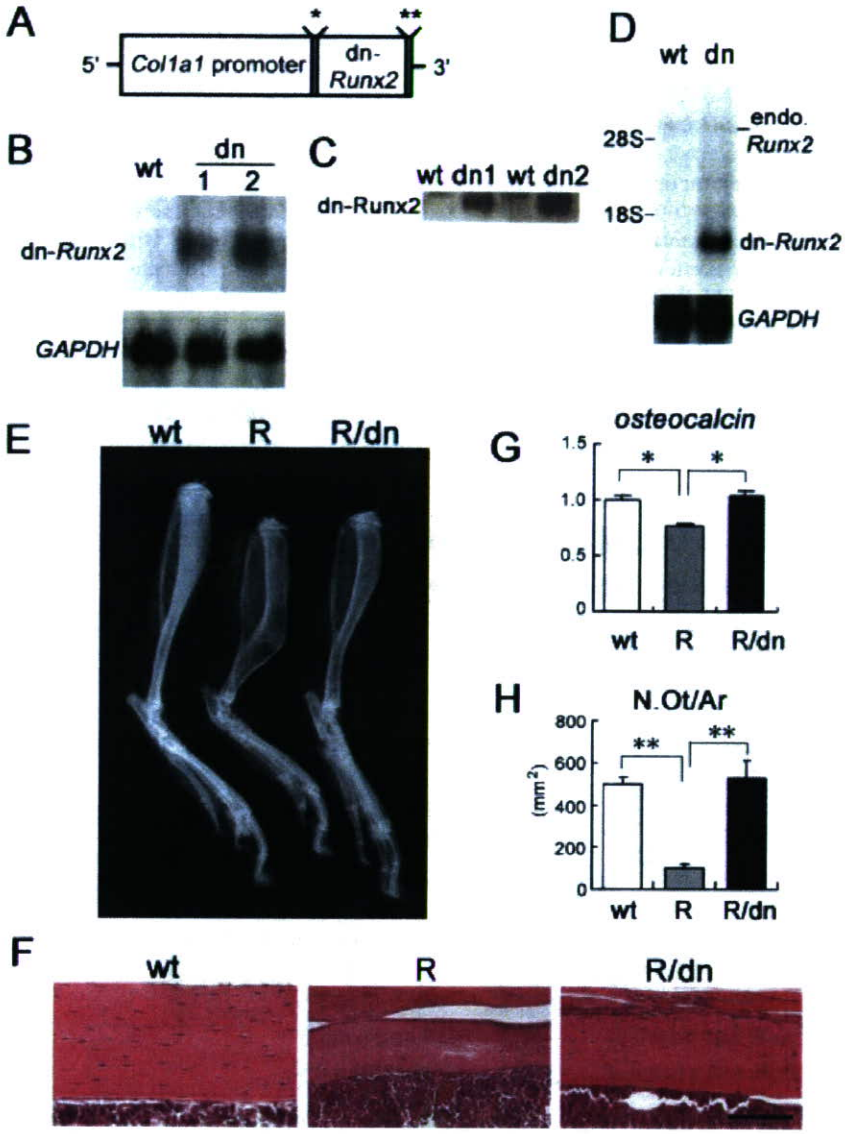

Fig. 2. Generation of dn-*Runx2* transgenic mice and *Runx2*/dn-*Runx2* double transgenic mice. **A:** Diagram of the DNA construct used to generate transgenic mice that express dn-*Runx2* under the control of the *Col1a1* promoter. *Intron from SV40 containing splice donor and acceptor sites, **polyadenylation signal from SV40. **B:** Northern blot analysis of the transgene. The expression level of the transgene was examined by Northern blot analysis using total RNA that had been extracted from the long bones of dn-*Runx2* transgenic mouse (dn) lines 1 and 2 and wild-type mice (wt) at birth. **C:** Western blot analysis of the transgene. Ten micrograms of nuclear extract from the calvaria of wild-type (wt) and two lines of dn-*Runx2* transgenic newborn mice (dn1 and dn2) was loaded in each lane and reacted with a polyclonal anti-Runx2 antibody that recognizes the N-terminus of type I Runx2. **D:** Comparison of the mRNA expression of endogenous *Runx2* and the transgene by Northern blot analysis. RNA was extracted from the long bones of wild-type mice (wt) and dn-*Runx2* transgenic mouse (dn) line 1 at 4 weeks of age. In B and D, 20 μg of total RNA was loaded and hybridized with ^{32}P-labeled cDNA of the *runt* region. *GAPDH* was used as an internal control. **E:** X-ray analysis of the long bones from a wild-type (wt), *Runx2* transgenic (R), and *Runx2*/dn-*Runx2* double transgenic (R/dn) mice at 6 weeks of age. The long bones of the *Runx2* transgenic mouse (R) are radiolucent compared with those of the wild-type mouse (wt) and have fractures in the tibia, fibula, and calcaneus. The long bones of the *Runx2*/dn-*Runx2* double transgenic mouse (R/dn) are mildly radiolucent but have no fracture. **F:** H-E staining of cortical bone in the tibiae of wild-type (wt), *Runx2* transgenic (R), and *Runx2*/dn-*Runx2* double transgenic (R/dn) mice at 6 weeks of age. The osteocyte number is drastically reduced in the *Runx2* transgenic mouse (R), whereas it is restored in the *Runx2*/dn-*Runx2* double transgenic mouse (R/dn). Scale bar = 100 μm. **G,H:** Northern blot analysis of osteocalcin expression (G) and the number of osteocytes (N.Ot/Ar) in cortical bone at the diaphyses of tibiae (H) of wild-type (wt), *Runx2* transgenic (R), and *Runx2*/dn-*Runx2* double transgenic (R/dn) mice. On Northern blot analysis, the intensity of each band was normalized against that of *GAPDH*, and the value in wild-type mice was defined as 1. Relative values are shown. Three mice in each group at 10 weeks of age were analyzed in G, and 4–6 mice in each group at 7 weeks of age were analyzed in H. *$P < 0.05$ and **$P < 0.01$.

teopenic phenotype of the double transgenic mice indicates that the expression level of dn-Runx2 was not high enough to inhibit exogenous Runx2 completely, because Runx2 and dn-Runx2 bound a Runx recognition sequence with similar efficiencies (unpublished data). These findings indicate that dn-*Runx2* expression inhibited Runx2 function in vivo and restored the late stage of osteoblast differentiation and their transition to osteocytes.

Age-Dependent Increase in Bone Mass in dn-*Runx2* Transgenic Mice

On X-ray and peripheral quantitative computed tomography (pQCT) analyses of long bones, the trabecular bone density of dn-*Runx2* transgenic mice and wild-type mice at 4 weeks of age did not significantly differ (Fig. 3A and B). However, the trabecular bone density was significantly higher in the dn-*Runx2* transgenic mice than in wild-type mice at 10 weeks and at 7 months of age. Histological analysis also showed an increased amount of trabecular bone in dn-*Runx2* transgenic mice at 7 months of age (Fig. 3E). The dn-*Runx2* transgenic mice showed transient reductions in the mineralization and volume of cortical bone, as shown by the reductions in mineral density and thickness compared with the respective values in wild-type mice, at 10 weeks of age (Fig. 3C and D).

In bone histomorphometric analysis, the trabecular bone volume (BV/TV) in dn-*Runx2* transgenic mice was similar to that in wild-type mice up through the young adult age (10 weeks of age) but it increased thereafter, and the trabecular bone volume in dn-*Runx2* transgenic mice was 50% higher than that in wild-type mice at 7 months of age (Fig. 4A). The thickness of newly deposited matrix (osteoid thickness; O.Th) was lower in dn-*Runx2* transgenic mice, with a significant difference seen at 10 weeks of age, and the osteoblast number (N.Ob/B.Pm) was significantly reduced at 4 weeks of age compared with those in the wild-type mice. The reduction in osteoblast number seemed to be caused by decreased osteoblast proliferation, because osteoblast prolifera-

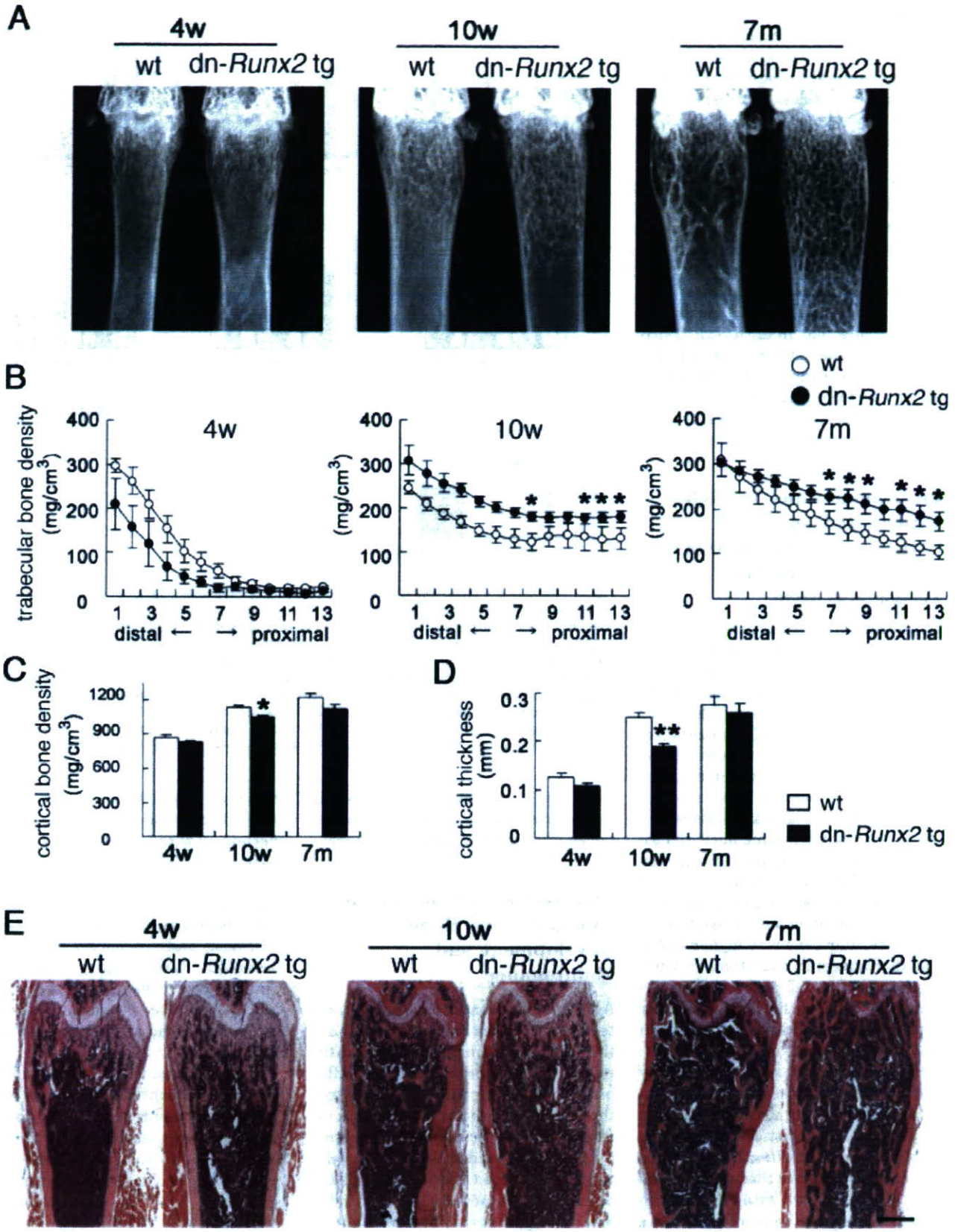

Fig. 3. X-ray, pQCT, and histological analyses of the distal femur of dn-*Runx2* transgenic mice at 4 weeks, 10 weeks, and 7 months of age. X-ray (**A**), pQCT (**B–D**), and histological (**E**) analyses of the distal femur of wild-type (wt) and dn-*Runx2* transgenic mice at 4 weeks, 10 weeks, and 7 months of age. The trabecular bone density in 13 equal cross-divisions of the metaphysial parts of the femurs was measured in wild-type (open circles) and dn-*Runx2* transgenic (closed circles) mice (B). The cortical bone density (C) and cortical thickness (D) of the diaphyses of the femurs were measured in wild-type (open columns) and dn-*Runx2* transgenic mice (closed columns). Data are presented as mean ± S.E. (n = 4–5). $^{*}P < 0.05$ and $^{**}P < 0.01$ between wild-type and transgenic mice. E: Sections were stained with H-E. Scale bar = 500 μm.

tion was increased in both type I and type II *Runx2* transgenic mice (Kanatani et al., 2006). Osteoclast parameters, including the eroded surface (ES/BS) and osteoclast number (N.Oc/B.Pm), were similar and bone formation rate (BFR/BS) was not significantly different between the dn-*Runx2* transgenic mice and wild-type mice. To determine the level of bone resorption, we examined the urinary deoxypyridinoline level, a marker of bone resorption, and found that it was significantly reduced in the dn-*Runx2* transgenic mice (Fig. 4B). These findings indicate that in dn-*Runx2* transgenic mice, the bone mass of the trabecular bone gradually increased with aging due to reduced bone resoption, even though the parameters of osteoclasts remained at normal levels.

Trabecular Bone Is Highly Mineralized and the Collagen Fibrils Are Densely Packed in dn-*Runx2* Transgenic Mice

To investigate the reason why bone resorption was reduced in dn-*Runx2* transgenic mice, we examined the characteristics of bone by transmission electron microscope (TEM) at 12 weeks of age (Fig. 5). Mineralization of matrix vesicles in the trabecular bone, which is typically observed in the mineralization of osteoid, was seen in wild-type mice (Fig. 5A). However, in the dn-*Runx2* transgenic mice, the osteoid was thin, the mineralization surface was flat, and mineralization of matrix vesicles was rarely seen (Fig. 5B). The extent of mineralization in the trabecular bone was higher in dn-Runx2 transgenic mice than in wild-type mice (Fig. 5C and D). Furthermore, the collagen fibrils were loosely deposited in a random orientation in the trabecular bone of wild-type mice, while they were densely and regularly packed in the trabecular bone of dn-*Runx2* transgenic mice (Fig. 5E and F). These characteristics of the trabecular bone of dn-*Runx2* transgenic mice were similar to those seen in the cortical bone of both wild-type and dn-*Runx2* transgenic mice (Fig. 5G and H, and data not shown). These findings indicate that the trabecular bone in dn-*Runx2* transgenic mice had characteristics of compact bone, which explains why bone resorption was reduced in dn-*Runx2* transgenic mice.

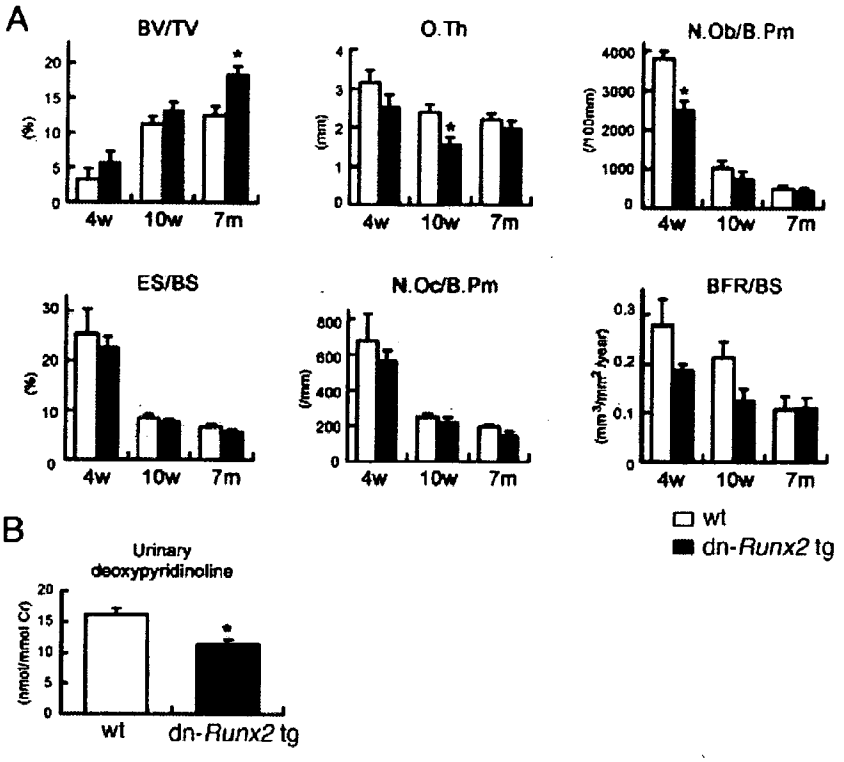

Fig. 4. Bone histomorphometric analyses and urinary deoxypyridinoline levels of dn-*Runx2* transgenic mice. **A:** Histomorphometric analyses. The trabecular bone volume (bone volume/tissue volume, BV/TV), osteoid thickness (O.Th), number of osteoblasts (N.Ob/B.Pm), eroded surface (ES/BS), number of osteoclasts (N.Oc/B.Pm), and bone formation rate (BFR/BS) were compared between wild-type (open columns) and dn-*Runx2* transgenic (closed columns) mice at 4 weeks, 10 weeks, and 7 months of age. The analyses were done on secondary spongiosa (0.75–1.5 mm from the growth plates) using the distal parts of femurs. **B:** Urinary deoxypyridinoline levels. The level of urinary deoxypyridinoline was examined in wild-type (wt) and dn-*Runx2* transgenic mice at 12 weeks of age. Bars show the mean ± S.E. of 4–5 mice in A and 7–10 mice in B. $^*P < 0.05$ between wild-type and dn-*Runx2* transgenic mice. B.Pm, bone perimeter; BS, bone surface.

Expression of Endogenous Runx2 During Bone Development and Maintenance

As the expression of dn-*Runx2* in osteoblasts resulted in the maturation of the trabecular bone, we examined the expression of endogenous Runx2 after birth in wild-type mice. We compared the *Runx2* expression with *Col1a1, osteopontin,* and *osteocalcin* expression by in situ hybridization using wild-type long bones (Fig. 6). Most of the osteoblasts at newborn stage and 1 week of age were immature and expressed *Col1a1, osteopontin,* and *Runx2,* while *osteocalcin*-positive mature osteoblasts were restricted to cortical bone (Fig. 6A–H). At 4 weeks of age, the expression pattern of *Runx2* overlapped with that of *osteopontin* or *osteocalcin* (Fig. 6I–L). At 8 weeks of age, *osteocalcin*-positive mature osteoblasts expressed *Runx2* moderately and *osteopontin* weakly (Fig. 6M–P), but *Runx2* and *osteopontin* expression decreased during aging and was faintly detected in many *osteocalcin*-positive mature osteoblasts at 12 weeks of age and at 10 months of age (Fig. 6Q–X).

We also examined the expression of Runx2, osteopontin, and osteocalcin proteins in wild-type mice by double labeling using anti-Runx2, anti-osteopontin, and anti-osteocalcin antibodies (Fig. 7). At 1 week of age, preosteoblasts in the periosteum of mandible expressed Runx2 but not osteopontin and osteocalcin (Fig. 7A–C, asterisks). Inside of mandible, however, both osteopontin-positive im-

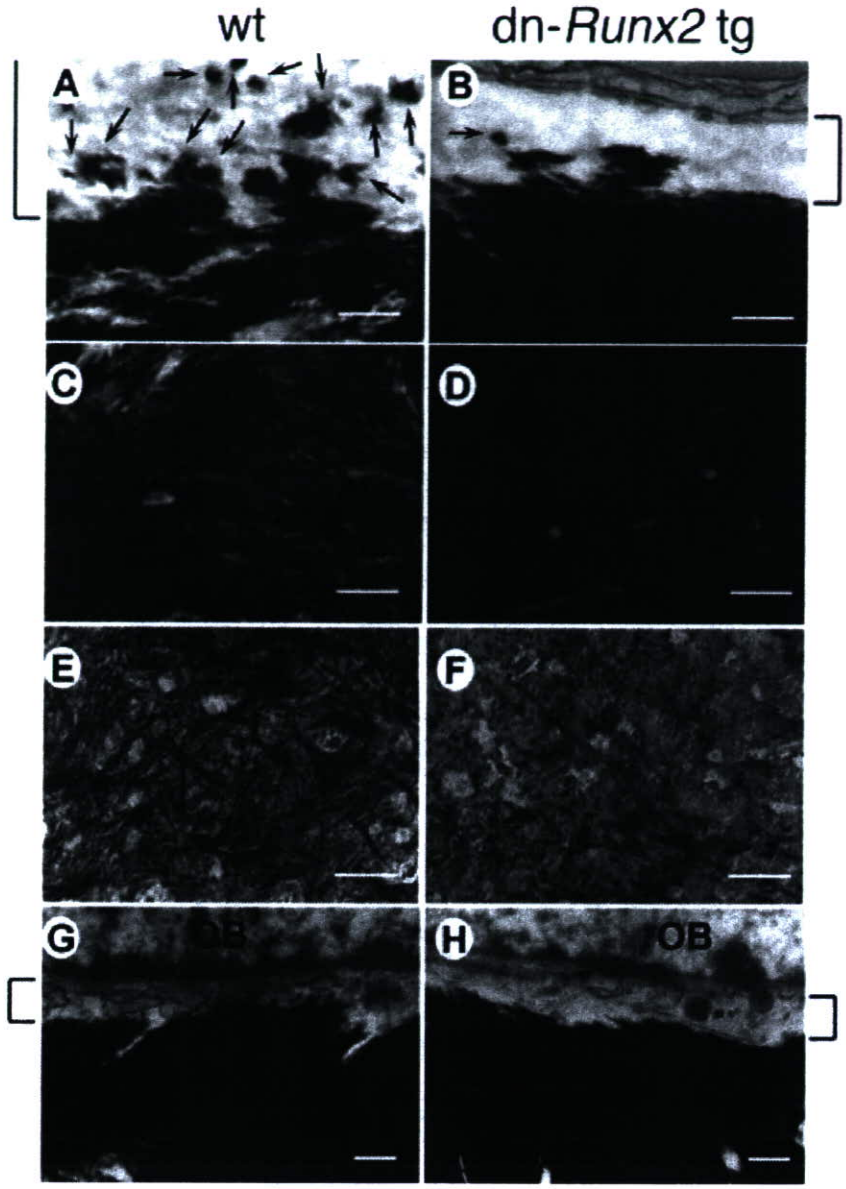

Fig. 5. Analysis of the characteristics of bone by TEM. Undecalcified (**A–D, G,H**) and decalcified (**E,F**) sections of trabecular bone (A–F) and cortical bone (G, H) from wild-type (A, C, E, G) and dn-*Runx2* transgenic (B, D, F, H) mice were examined by TEM at 12 weeks of age. A–D: Structure of trabecular bone. Mineralized matrix vesicles are shown by arrows in A and B. E,F: Collagen fibrils in trabecular bone. G,H: Structure of cortical bone. OB, osteoblast. Calcified bone matrix is seen in black in A–D, G, and H. Osteiod is shown in brackets in A, B, G, and H. Scale bars = 1 μm.

mature osteoblasts and osteocalcin-positive early mature osteoblasts expressed Runx2 (Fig. 7B, arrows; Fig. 7C, arrowheads). In the femur, preosteoblasts in the perichondrial region surrounding proliferating and prehypertrophic chondrocytes expressed Runx2 but not osteopontin and osteocalcin (Fig. 7D–F, asterisks). Immature osteoblasts surrounding the hypertrophic chondrocyte layer expressed Runx2 and osteopontin but not osteocalcin (Fig. 7E, arrows). Osteocalcin-positive early mature osteoblasts, which expressed Runx2, appeared in the metaphyseal cortical bone (Fig. 7F, arrowhead). In the diaphysis of the femur, both osteopontin-positive immature osteoblasts and osteocalcin-positive early mature osteoblasts expressed Runx2 (Fig. 7H, arrows; 7I, arrowheads). In the metaphysis of femur at 4 weeks of age, osteopontin-positive immature osteoblasts strongly expressed Runx2, while osteocalcin-positive mature osteoblasts weakly expressed Runx2 (Fig. 7K, arrows; 7L, arrowheads). In the diaphysis, we observed an apparent reduction in Runx2 and osteopontin protein expression compared with their mRNA expression (Fig. 6), and Runx2 and osteopontin proteins were barely detectable in most of the osteocalcin-positive late mature osteoblasts (Fig. 7M–O, arrows). These findings show that Runx2 is expressed in preosteoblasts, in which osteopontin and osteocalcin are not expressed, is strongly expressed in osteopontin-positive immature osteoblasts, and then is expressed in osteocalcin-positive early mature osteoblasts, but that Runx2 expression is reduced in osteocalcin-positive late mature osteoblasts.

Expression of Major Bone Matrix Protein Genes in the Osteoblasts of dn-*Runx2* Transgenic Mice Was Not Impaired

We examined the expression of bone matrix protein genes including *Col1a1*, *osteopontin*, and *osteocalcin* by Northern blot analysis and in situ hybridizatoin. *Col1a1* and *osteocalcin* expression were significantly reduced and *osteopontin* expression was marginally reduced in the dn-*Runx2* transgenic mice at 4 weeks of age (Fig. 8A–C). However, it is considered that the reduced expression levels of these matrix protein genes were mainly due to the reduced number of osteoblasts in dn-*Runx2* transgenic mice, because their expression decreased in parallel with the reduction in the number of osteoblasts at 4 weeks of age (Figs. 4A, 8A–C). In situ hybridization analysis confirmed that there were

Fig. 6. Expression of bone matrix protein genes and *Runx2* in postnatal bone development and maintenance. The expression of *Col1a1* (**A, E, I, M, Q, U**), *osteopontin* (**B, F, J, N, R, V**), *osteocalcin* (**C, G, K, O, S, W**), and *Runx2* (**D, H, L, P, T, X**) was examined by in situ hybridization at newborn stage (A–D) and 1 week (E–H), 4 weeks (I–L), 8 weeks (M–P), 12 weeks (Q–T), and 10 months (U–X) of age. Serial sections from femur (A–D) and tibiae (E–X) were used for in situ hybridization. Arrow in X indicates faint expression of Runx2. Scale bars = 100 μm.

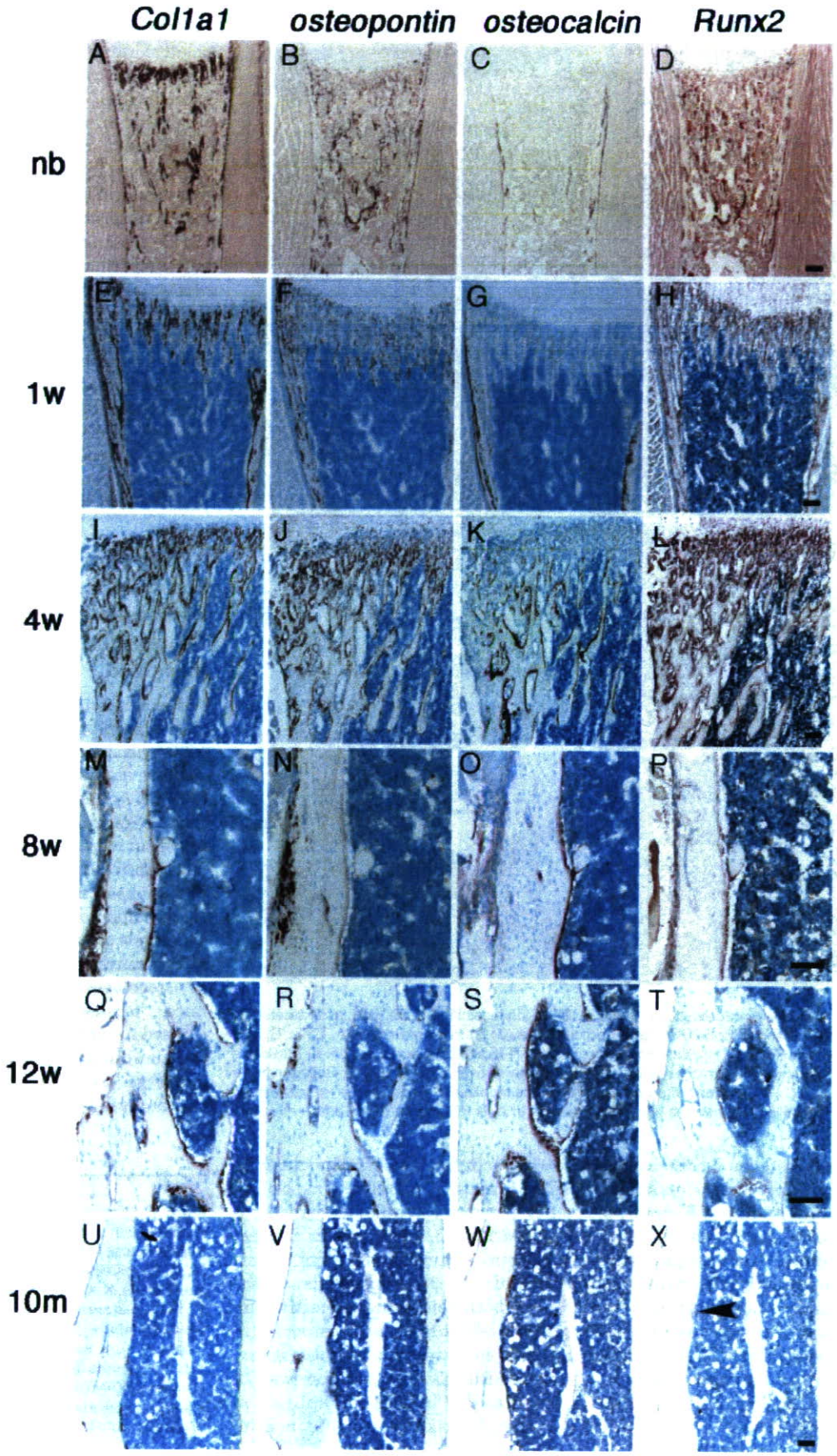
Col1a1
osteopontin
osteocalcin
Runx2
nb
1w
4w
8w
12w
10m
A
B
C
D
E
F
G
H
I
J
K
L
M
N
O
P
Q
R
S
T
U
V
W
X

Fig. 6.

reduced numbers of *Col1a1*-positive, *osteopontin*-positive, and *osteocalcin*-positive cells at 4 weeks of age (Figs. 8D–I). At 10 weeks of age, the dn-*Runx2* transgenic mice expressed similar levels of *Col1a1*, *osteopontin*, and *osteocalcin* compared with the respective levels in wild-type mice as demonstrated by Northern blot analysis (Fig. 8A–C) and in situ hybridization (Fig. 8J–O). These findings showed that individual osteoblasts in dn-*Runx2* transgenic mice expressed these matrix protein genes at nearly normal levels, and indicate that Runx2 is not absolutely required for maintenance of the expression of the major bone matrix protein genes in postnatal bone development and maintenance.

The expression levels of *RANKL* and *OPG*, which stimulate and inhibit osteoclast differentiation, respectively, did not significantly differ between the dn-*Runx2* transgenic mice and wild-type mice at 4 and 10 weeks of age by real-time reverse transcription (RT)-PCR (Fig. 8P, Q).

Bone Resorption Was Not Enhanced After Ovariectomy in dn-*Runx2* Transgenic Mice

As bone resorption was reduced in dn-*Runx2* transgenic mice, the response of the trabecular bone to estrogen depletion was investigated. We performed ovariectomy at 4 months of age, and examined the urinary deoxypyridinorine level one week later (Fig. 9A). Although there was no significant difference in the urinary deoxypyridinorine level between wild-type and dn-*Runx2* transgenic mice that underwent a sham operation, probably due to an increase in bone mass in dn-*Runx2* transgenic mice at this age, the urinary deoxypyridinoline level in ovariectomized wild-type mice was significantly higher than those in sham-operated wild-type mice and ovariectomized dn-*Runx2* transgenic mice. In contrast, the urinary deoxypyridinoline levels were similar between sham-operated and ovariectomized dn-*Runx2* transgenic mice. Five weeks after ovariectomy, the femurs were compared with those from sham-operated mice by X-ray, pQCT, and bone morphometric analyses. After ovariectomy, the trabecular mineral content of femurs apparently decreased in wild-type mice but not in dn-*Runx2* transgenic mice (Fig. 9B–D). The eroded surface, osteoclast surface, and osteoclast number were significantly higher and the bone formation rate was marginally higher after ovariectomy in the wild-type mice, although these parameters did not significantly change after ovariectomy in the dn-*Runx2* transgenic mice (Fig. 9E–H). These results show that ovariectomy did not enhance bone resorption nor bone formation in dn-*Runx2* transgenic mice.

As bone resorption was not enhanced after ovariectomy in dn-*Runx2* transgenic mice, we examined the function of Runx2 in osteoclastogenesis by coculture of calvarial cells and bone marrow cells. Adenoviral introduction of *Runx2* to wild-type calvarial cells increased TRAP-positive cells and resorbed area, while adenoviral introduction of dn-*Runx2* reduced them, indicating that Runx2 positively regulates osteoclast differentiation and bone resorption (Fig. 9I–K).

These findings suggest that Runx2 induces bone loss in the estrogen-deficient state not only by regulating bone maturity but also by mediating the enhancement of osteoclastogenesis after estrogen depletion.

Less Anabolic Effect of Parathyroid Hormone (PTH) in dn-*Runx2* Transgenic Mice

To examine the effect of PTH in dn-*Runx2* transgenic mice, we injected rat PTH(1-34) three times a day at a dose of 80 μg/kg for 18 days. A previous report showed that the same protocol using human PTH(1-34) decreased bone mineral density in rats (Frolik et al., 2003). After the treatment with PTH, however, we observed significant increases in trabecular bone volume, trabecular number, trabecular thickness, and cortical bone volume in wild-type mice (Fig. 10). In dn-*Runx2* transgenic mice, trabecular bone volume and thickness increased after the PTH treatment, but the increase in the trabecular bone volume was less than that of wild-type mice and the trabecular number and cortical bone volume were not increased (Fig. 10B–E). These findings indicate that the osteoblasts in dn-*Runx2* transgenic mice are less responsive to the anabolic effect of PTH, suggesting that Runx2 is involved in the anabolic effect of PTH. The involvement of Runx2 in the anabolic effect of PTH was also reported previously (Krishnan et al., 2003).

DISCUSSION

We investigated the function of Runx2 in osteoblasts using dn-*Runx2* in in vitro and in vivo studies. Adenoviral introduction of dn-*Runx2* suppressed ALP activity in immature mesenchymal cells, but it did not suppress *osteocalcin* and *Col1a1* expression in mature osteoblastic cells in vitro. In *Runx2* transgenic mice, dn-Runx2 restored osteoblast differentiation at the late stage and their transition to osteocytes, which were inhibited in *Runx2* transgenic mice. Dn-*Runx2* transgenic mice showed increased mineralization and increased volume of the trabecular bone, and the trabecular bone had the appearance of compact bone. These findings indicate that dn-Runx2 increased the volume of trabecular bone by promoting the formation of mature bone, which is relatively resistant to bone resorption. In accordance with these findings, endogenous Runx2 was highly expressed in immature osteoblasts but downregulated during osteoblast maturation in wild-type mice. Furthermore, dn-Runx2 conserved the trabecular bone after estrogen depletion by promoting bone maturation as well as inhibiting osteoclastogenesis. Moreover, dn-*Runx2* transgenic mice showed less response to the anabolic effect of PTH. Thus, the level of Runx2 determines bone maturity and the bone turnover rate, and is responsible for the bone loss observed in the estrogen-deficient state and at least partly for the anabolic effect of PTH. However, as the expression levels of major bone matrix protein genes in individual osteoblasts of the dn-*Runx2* transgenic mice were not significantly reduced, our findings also indicate that Runx2 is not essential for maintenance of the expression of major bone matrix protein genes in postnatal bone development and maintenance.

In dn-*Runx2* transgenic mice, the trabecular bone had characteristics of compact bone, in that the bone was highly

mineralized and collagen fibrils were densely and regularly deposited, and the trabecular bone was refractory to bone resorption. In contrast, the cortical bone of *Runx2* transgenic mice is mainly composed of less mineralized, immature bone, so-called woven bone, in which collagen fibers run in all directions, and is prone to bone resorption (Liu et al., 2001; Geoffroy et al., 2002). Furthermore, Runx2 was strongly expressed in immature osteoblasts but downregulated during osteoblast maturation in wild-type mice (Figs. 6, 7). In postnatal bone development, therefore, Runx2 plays an important role in maintaining a supply of immature osteoblasts, leading to the formation of immature bone that is easily resorbed, whereas Runx2 has to be suppressed for osteoblast differentiation at the late stage and compact bone formation. Thus, bone maturity and the bone turnover rate are determined by the level of functional Runx2. In contrast to our present finding that suppression of Runx2 in osteoblastic cells resulted in an increase in trabecular bone volume, selective deficiency of a Runx2 isoform (type II Runx2) results in severe osteopenia (Xiao et al., 2005), indicating that insufficiency of Runx2 at the beginning of osteoblast differentiation leads to osteopenia in which both bone formation and bone resorption are reduced with more severe impairment in bone formation.

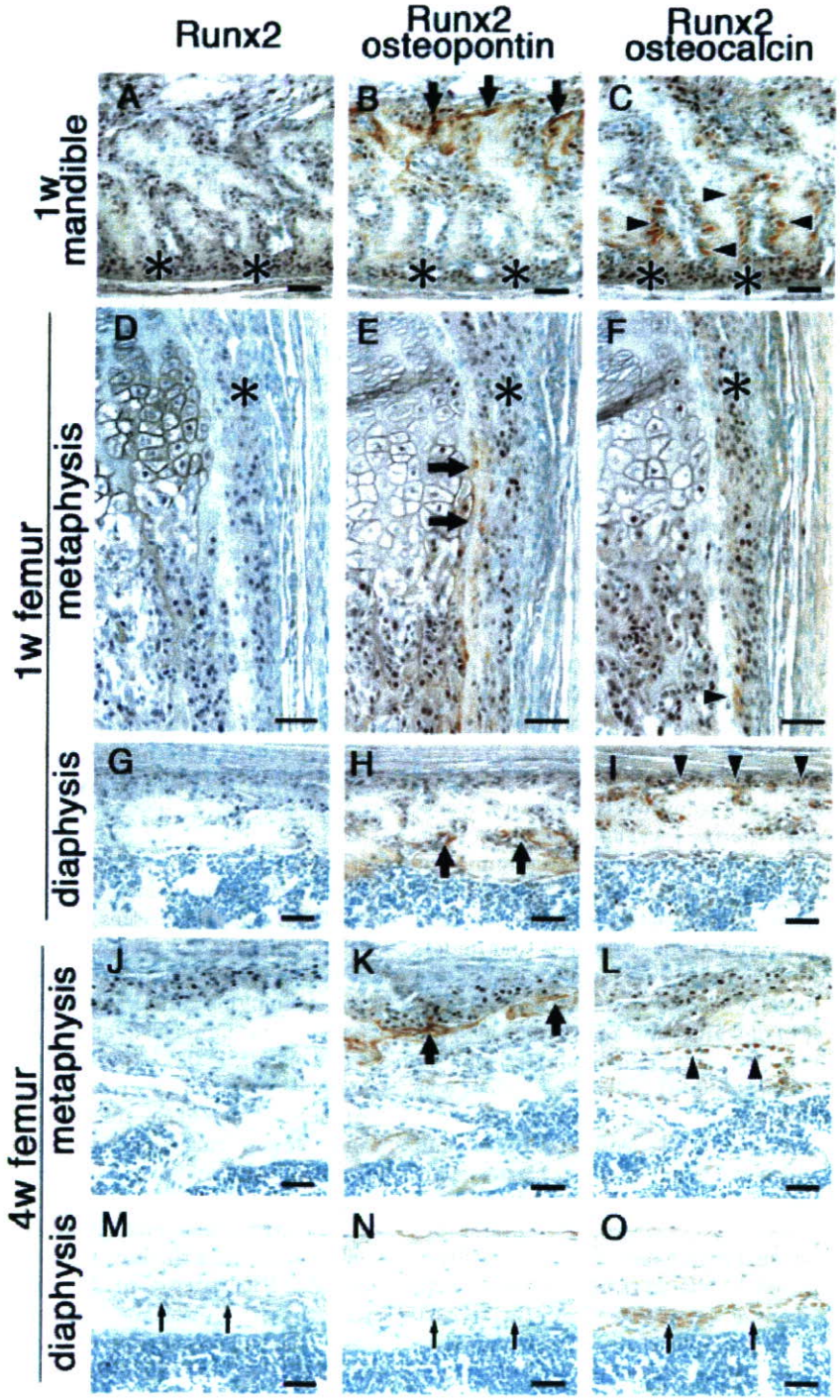

Fig. 7.

Fig. 7. Expression of Runx2, osteopontin, and osteocalcin proteins during bone development. Single labeling with anti-Runx2 antibody (**A, D, G, J, M**), double labeling with anti-Runx2 and anti-osteopontin antibodies (**B, E, H, K, N**), and double labeling with anti-Runx2 and anti-osteocalcin antibodies (**C, F, I, L, O**) are shown. The single labeling with anti-osteopontin or anti-osteocalcin antibody is not shown here. The labeling with anti-Runx2 antibody is stained black, and the labeling with anti-osteopontin or anti-osteocalcin antibody is stained brown. The sections were counterstained with methyl green. A–C: Serial sections from mandible at 1 week of age. Asterisks indicate preosteoblasts in periosteum, arrows indicate osteopontin-positive immature osteoblasts, and arrowheads indicate osteocalcin-positive early mature osteoblasts. The bone matrix was also stained strongly by osteopontin and weakly by osteocalcin. D–I: Serial sections from femurs at 1 week of age. D–F: The region from perichondrium to the cortical bone at metaphysis is shown. Asterisks indicate preosteoblasts in the perichondrium, arrows indicate osteopontin-positive immature osteoblasts, and the arrowhead indicates osteocalcin-positive early mature osteoblasts. G–I: Cortical bones at diaphysis are shown. Arrows indicate osteopontin-positive immature osteoblasts, and arrowheads indicate osteocalcin-positive early mature osteoblasts. J–O: Serial sections from femurs at 4 weeks of age. J–L: Cortical bones at metaphysis are shown. Arrows indicate osteopontin-positive immature osteoblasts, and arrowheads indicate osteocalcin-positive mature osteoblasts. Runx2 is strongly expressed in osteopontin-positive osteoblasts and weakly in osteocalcin-positive osteoblasts. M–O: Cortical bones at diaphysis are shown. Arrows indicate osteocalcin-positive late mature osteoblasts, in which Runx2 and osteopontin are barely detectable. No signal was detected by immunohistochemistry in the absence of treatment with the first antibodies (data not shown). Scale bars = 50 μm.

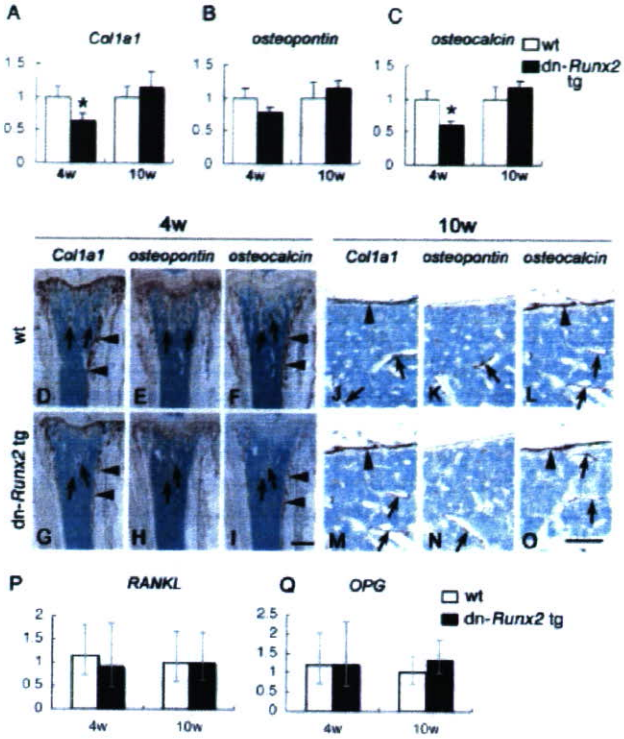

Fig. 8. Analysis of the expression of genes encoding bone matrix proteins, endogenous *Runx2*, and genes involved in osteoclastogenesis. RNA was extracted from the long bones at 4 and 10 weeks of age for Northern blot analysis (**A–C**) and real-time RT-PCR (**P, Q**). Twenty micrograms of total RNA was loaded in each lane and hybridized with probes of *Col1a1* (A), *osteopontin* (B), or *osteocalcin* (C). *GAPDH* was used as an internal control. The intensity of each band was normalized against that of *GAPDH*, the value in wild-type mice was defined as 1, and relative values are shown (A–C). The data are shown as the mean ± S.E. of 5–6 mice. * vs. wild-type mice. $^*P < 0.01$. **D–O:** To examine the expression of bone matrix protein genes, sections of the tibiae of wild-type (wt) (D–F, J–L) and dn-*Runx2* transgenic (G–I, M–O) mice at 4 weeks (D–I) and 10 weeks (J–O) of age were subjected to in situ hybridization using *Col1a1* (D, G, J, M), *osteopontin* (E, H, K, N), and *osteocalcin* (F, I, L, O) probes. At 4 weeks of age, the numbers of *Col1a1*-positive cells and *osteocalcin*-positive cells in the trabecular bone (arrows) and cortical bone (arrowheads) are apparently lower (D, F, G, I), and the number of *osteopontin*-positive cells in trabecular bone (arrows) is mildly reduced in the dn-*Runx2* transgenic mouse compared with wild-type mouse (E, H). The expression levels of *Col1a1*, *osteocalcin*, and *osteopontin* are similar between wild-type and dn-*Runx2* transgenic mice in both the trabecular bone (arrows) and endosteum (arrowheads) at 10 weeks of age. Scale bars = 500 μm; (D–I); 100 μm (J–O). The expression of *RANKL* (P) and *OPG* (Q) were examined in wild-type and dn-*Runx2* transgenic mice by real-time RT-PCR. The values of wild-type mice at 10 weeks of age were defined as 1, and relative levels are shown. Data represent mean of 4–8 mice. Open columns, wild-type mice; closed columns, dn-*Runx2* transgenic mice.

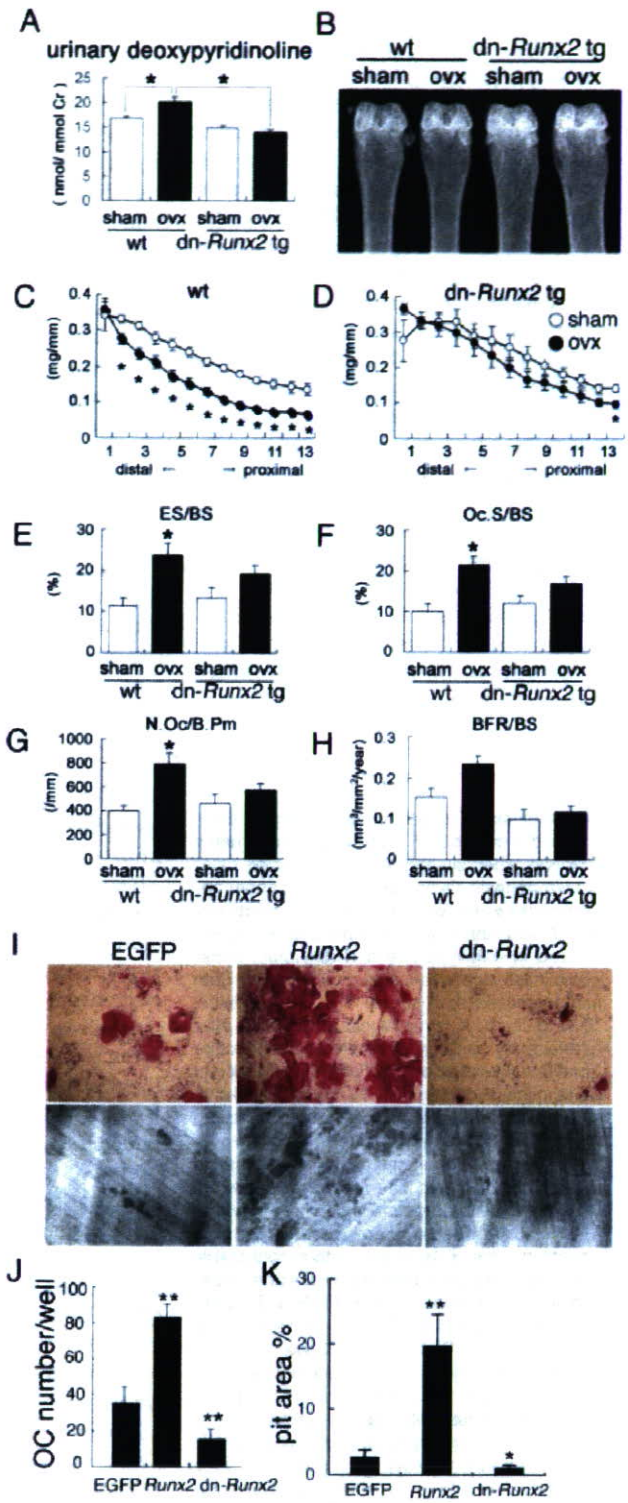

Fig. 9.

Runx2 is considered to play important roles in the regulation of expression of major bone matrix protein genes including *Col1a1, osteopontin, bone sialoprotein*, and *osteocalcin* and in postnatal bone development (Ducy et al., 1997, 1999; Sato et al., 1998; Harada et al., 1999; Javed et al., 1999; Kern et al., 2001). Adenoviral introduction of *Runx2* in mature osteoblastic cells in vitro up-regulated *osteocalcin* expression but not *Col1a1* expression, while adenoviral introduction of dn-*Runx2* did not suppress the expression of *Col1a1* nor *osteocalcin*, which were highly expressed in the mature osteoblastic cells (Fig. 1F–H). These findings, combined with previous

findings, indicate that Runx2 is able to up-regulate the expression of major bone matrix protein genes in osteoblastic cells and in immature mesenchymal cells, although Runx2 is not absolutely required for the steady-state expression of these genes in mature osteoblastic cells. Moreover, the expression levels of major bone matrix protein genes in individual osteoblasts of dn-*Runx2* transgenic mice were not reduced (Figs. 4A and 8A–C). Therefore, our findings indicate that Runx2 is not essential for maintenance of the expression of major bone matrix protein genes in mature osteoblasts in postnatal bone development and maintenance. The down-regulation of endogenous Runx2 during osteoblast maturation also supports the conclusion (Figs. 6, 7). As Runx2 induces the expression of major bone matrix protein genes in immature mesenchymal cells in vitro (Ducy et al., 1997; Harada et al., 1999), however, it is likely that Runx2 triggers the expression of these genes in mesenchymal progenitors in vivo.

Interestingly, the trabecular bone in dn-*Runx2* transgenic mice did not significantly decrease after ovariectomy (Fig. 9B–D). In the trabecular bone, neither the parameters of bone resorption nor bone formation were enhanced in dn-*Runx2* transgenic mice after ovariectomy (Fig. 9A,E–H), indicating that Runx2 is highly involved in the high bone turnover in the estrogen-deficient state. It is considered that the trabecular bone was conserved after ovariectomy in dn-*Runx2* transgenic mice due to its compact bone-like structure and the absence of enhancement of osteoclastogenesis. We previously reported that *in vitro* Runx2 induces *RANKL* expression and inhibits *OPG* expression in calvarial cells derived from *Runx2* null (−/−) mice (Enomoto et al., 2003). However, we could not detect evidence that Runx2 regulated *RANKL* and *OPG* expression in either *Runx2* or dn-*Runx2* transgenic mice (Liu et al., 2001) (Fig. 8P,Q). These findings suggest that Runx2 regulates *RANKL* and *OPG* expression only during the differentiation stage of mesenchymal cells. Dn-*Runx2* expression in osteoblastic cells suppressed osteoclastogenesis after ovariectomy (Fig. 9E–G). However, the molecular mechanisms through which Runx2 mediates the enhancement of osteoclastogenesis in the estrogen-depleted state need to be further investigated. Estrogen inhibits osteoclastogenesis, and the estrogen receptor α interacts with Runx2, enhancing transcriptional activation by Runx2 (Manolagas and Jilka, 1995; Pacifici, 1996; McCarthy et al., 2003). As Runx2 was involved in the enhancement of osteoclastogenesis and bone resorption after ovariectomy (Fig. 9), estrogen seems to inhibit osteoclastogenesis through a mechanism other than Runx2-dependent transcriptional activation. As our findings indicate that Runx2 is responsible for bone loss in the estrogen-deficient state, dn-*Runx2* transgenic mice will be a useful model for the study of mechanisms involved in the development of menopausal osteoporosis.

Fig. 9. Quantification of urinary deoxypyridinoline and X-ray, pQCT, and histomorphometric analyses after ovariectomy and in vitro osteoclastogenesis. Ovariectomy (ovx) or sham operation (sham) was performed at 4 months of age. **A:** Urinary deoxypyridinoline level was examined in wild-type (wt) and dn-*Runx2* transgenic mice one week after ovariectomy. Data are presented as mean ± S.E. of 6–8 mice. $^{*}P < 0.01$. **B:** X-ray analysis at 5 weeks after ovariectomy. **C,D:** pQCT analysis of trabecular bone 5 weeks after ovariectomy. The trabecular bone mineral contents in 13 equal cross-divisions of the metaphysial part of the distal femurs from ovariectomized (closed circles) or sham-operated (open circles) wild-type (C) and dn-*Runx2* transgenic (D) mice were compared. Data are presented as mean ± S.E. of 8 mice. $^{*}P < 0.05$ between ovariectomized and sham-operated mice. **E-H:** Bone histomorphometric analyses of trabecular bone 5 weeks after ovariectomy. The eroded surface (ES/BS) (E), osteoclast surface (Oc.S/BS) (F), number of osteoclasts (N.Oc/B.Pm) (G), and bone formation rate (BFR/BS) (H) were compared. Data are presented as mean ± S.E. of 6 mice. * vs. wild-type mice that underwent sham operation. $^{*}P < 0.01$. **I:** TRAP staining (top) and stained dentin slices (bottom). Wild-type calvarial cells were infected at a MOI of 10 with adenovirus expressing either EGFP, *Runx2*-EGFP (*Runx2*), or dn-*Runx2*-EGFP (dn-*Runx2*), and cultured with bone marrow cells for 6 days. **J:** Number of multinucleated TRAP-positive cells. **K:** Pit area. Multinucleated TRAP-positive cells and resorbed area were increased by overexpression of *Runx2* but reduced by dn-*Runx2*. Data are presented as mean ± S.D. of 12 wells. *vs. EGFP-expressing cells. $^{**}P < 0.001$, $^{*}P < 0.05$.

EXPERIMENTAL PROCEDURES

Cell Culture and Adenoviral Transfer

Mouse immature mesenchymal cell lines C2C12 and C3H10T1/2 and the mouse pre-osteoblastic cell line MC3T3-E1 were purchased from RIKEN Cell Bank (Tsukuba, Japan). Mouse mature osteoblastic cell line MLO-A5 was provided by Dr. Lynda Bonewald (The University of Texas Health Science Center, San Antonio, TX). Primary calvarial cells derived from mouse embryonic day 18.5 embryos were prepared as described previously (Komori et al., 1997). To induce osteoblast differentiation of primary calvarial cells and MC3T3-E1 cells, the medium was supplemented with 10 mM β-glycerophosphate and 100 μg/ml ascorbic acid. To induce osteoblast differentiation of C2C12 cells, the cells were treated with recombinant human BMP-2 (rhBMP-2) (100 ng/ml), which was provided by Yamanouchi Pharmaceutical Co. Ltd (Tokyo, Japan). Adenovirus vectors expressing type II *Runx2*, dn-*Runx2* (short form), dn-*Runx2* (long form), or EGFP were generated as previously described (Enomoto et al., 2003). Cells plated in collagen-coated 24-well plates were incubated with adenovirus for 2 hr. The infected cells were cultured for 7 days and stained for ALP as previously described (Komori et al., 1997).

Reporter Assay

Type II *Runx2*, dn-*Runx2* (short form) that contains the *runt* domain and the nuclear localization sequence, and dn-*Runx2* (long form) that contains the *runt* domain with the N-terminal domain of type I *Runx2* and the nuclear localization sequence, were subcloned into the pSG5 vector (Stratagene, La Jolla, CA). A pGL3 vector containing 6 repeats of the consensus Runx2 binding sequence (6 × OSE2) was used as the reporter vector (Harada et al., 1999). pRL-CMV was used as a control vector. Each expression vector (3 ng), the reporter vector (200 ng), and the control vector (2 ng) were cotransfected into C3H10T1/2 cells in 48-well multiplates using FuGENE 6 (Roche Diagnostics). An increasing amount of each dn-*Runx2* expression vector, 200

ng of the reporter vector, and 2 ng of the control vector were cotransfected into stable C3H10T1/2 transfectants of type II *Runx2*. The total amount of DNA for transfection was adjusted to 250 ng using an empty pSG5 vector. After 48 hr, the luciferase activity of the cell lysate was assayed using the Luciferase Reporter Assay System (Promega, Madison, WI). The transfection efficiency was normalized by quantifying *renilla* luciferase activity.

Generation of dn-*Runx2* Transgenic Mice and *Runx2*/dn-*Runx2* Double Transgenic Mice

To generate transgenic mice with osteoblasts that express dn-*Runx2*, dn-*Runx2* cDNA (long form) was inserted into the mammalian expression vector pNASSβ (CLONTECH) by replacing the β-galactosidase gene at the Not I sites, and the 2.3-kb osteoblast-specific promoter region of mouse *Col1a1* (Rossert et al., 1995) was inserted into pNASSβ at the XhoI site. The DNA fragment containing the 2.3-kb *Col1a1* promoter, an intron from SV40, dn-*Runx2* cDNA, and polyadenylation signal from SV40, was injected into the pronuclei of fertilized eggs from C57BL/6 X C3H F_1 (B6C3H F_1) mice. Transgene integration and expression were identified by Southern blot and Northern blot analyses, respectively, using the cDNA coding the *runt* domain of *Runx2* as a probe. Transgenic lines were maintained in a B6C3H F_1 background. The dn-*Runx2* transgenic mice were mated with transgenic mice that expressed *Runx2* under the control of the *Col1a1* promoter (Liu et al., 2001) to generate *Runx2*/dn-*Runx2* double transgenic mice. To investigate the effect of estrogen deficiency on bone, dn-*Runx2* transgenic mice and their wild-type littermates at 4 months of age were ovariectomized or sham-operated and sacrificed at 5 weeks after the surgery. The urinary excretion of deoxypyridinoline was measured using an ELISA kit (Metra Biosystems). Results were expressed as deoxypyridinoline/creatinine (nmol/mmolCr). Prior to the study, all experiments were reviewed and approved by the Animal Care and Use Committee of Nagasaki University Graduate School of Biomedical Sciences.

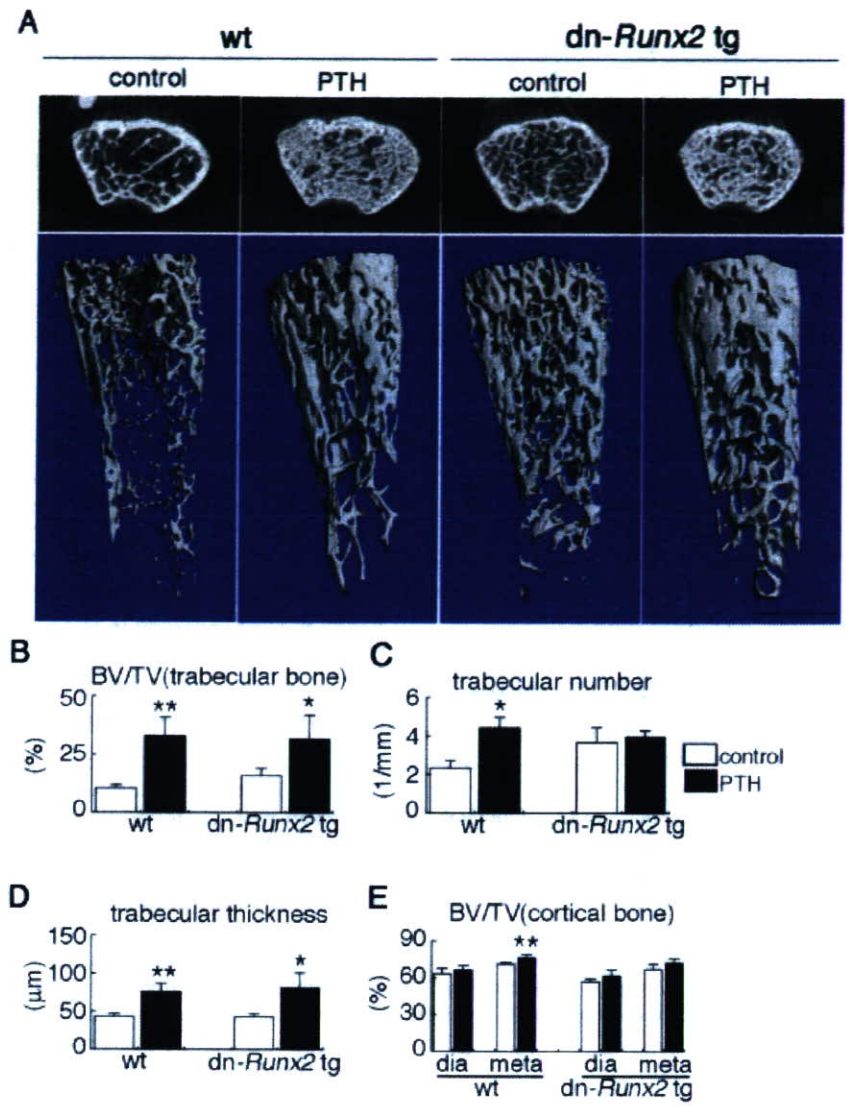

Fig. 10. Micro-CT analysis after PTH treatment. After 18 days of treatment with PTH or vehicle (control), 13-week-old wild-type (wt) and dn-*Runx2* transgenic (dn-*Runx2* tg) mice femurs were analyzed by micro-CT. **A:** Two-dimensional axial image of distal femoral metaphysis (top) and three-dimensional trabecular bone architecture of distal femoral metaphysis (bottom, scale bar = 1 mm). **B:** Trabecular bone volume (BV/TV). **C:** Trabecular number. **D:** Trabecular thickness. **E:** Cortical bone volume (BV/TV). Trabecular bone parameters were measured on distal femoral metaphysis, and cortical bone volume was measured on femoral diaphysis (dia) and proximal metaphysis (meta). Data are presented as mean ± S.D. of 5–10 mice. * vs. control. $^{**}P < 0.001$, $^{*}P < 0.05$.

Real-Time PCR and Northern Blot Analyses

Real-time PCR was performed using cDNA (7.5 ng total RNA equivalent) and the following primers as previously described (Enomoto et al., 2004): *RANKL*, 5′-CAAGCTCCGAGCTGGTGAAG-3′ and 5′-CCTGAACTTTGAAAGCCCCA-3′; *OPG*, 5′-AAGAGCAAACCTTCCAGCTGC-3′ and 5′-CACGCTGCTTTCACAGAGGTC-3′. We normalized the obtained CT (cycle number at which amplification threshold of detection was reached) values to that of rodent *Gapdh* (Applied Biosystems) expression by the ΔΔCT method. The mean ΔΔCT was converted to relative expression value by the equation, $2^{-\Delta\Delta Ct}$, and the range was calculated by the

equation, $2^{(-\Delta\Delta Ct+StdevAACt)}$. Northern blot analysis was performed using cDNA probes of *runt, Col1a1, osteopontin, osteocalcin*, and *GAPDH* as previously described (Inada et al., 1999). The relative intensities of the bands were measured using NIH Image software.

Western Blot Analysis

Nuclear extracts were prepared from the maxillae and mandibles of newborn mice using NE-PER reagent (Pierce). Proteins (10 μg/well) were resolved by SDS-12/25% gradient polyacrylamide gel electrophoresis. The blots were first incubated with a polyclonal rabbit antibody against the N-terminal domain of type I Runx2 (Ueta et al., 2001), and then with horseradish peroxidase-conjugated anti-rabbit IgG (New England Biolabs).

X-ray and pQCT Analyses

Long bones were dissected from sacrificed mice and subjected to X-ray exposure using a Micro-FX1000 (Fuji Film Inc., Tokyo, Japan). For pQCT analysis, femurs were fixed with 70% ethanol and analysis was performed using an XCT Research SA (Stratec Medizintechnick). Parameters of the trabecular bone and cortical bone were analyzed using the threshold value, 395 and 690 mg/cm^3, respectively.

Histological Analysis

For histological analyses of the long bones, mice were sacrificed at newborn stage, 1 week, 4 weeks, 8 weeks, 10 weeks, 12 weeks, 7 months, and 10 months of age. To prepare the sections for hematoxylin and eosin (H-E) staining and in situ hybridization, mice were fixed in 4% paraformaldehyde/0.1M phosphate buffer, and the long bones were decalcified in 0.5M EDTA/10% glycerol buffer (pH 7.5) and embedded in paraffin. Sections (7 μm thick) were stained with H-E or subjected to in situ hybridization using probes for *Col1a1, osteopontin, osteocalcin*, and *Runx2* as described previously (Inada et al., 1999). For assessment of dynamic histomorphometric indices, mice were injected twice with calcein at a dose of 0.16 mg/10 g body weight, and analysed at 4 weeks, 10 weeks, or 7 months of age, or at 5 weeks after ovariectomy. The mice received the two injections at 6 and 2 days before sacrifice. The long bones were fixed with 70% ethanol, and the undecalcified bones were embedded in glycolmethacrylate. Three-micrometer–thick longitudinal sections from the distal parts of femurs were stained with toluidine blue and analyzed using a semiautomated system (Bone Histomorphometric System, System Supply). For ultrastructural analysis, specimens were immersed in a mixture of 2% paraformaldehyde and 2.5% glutaraldehyde in 0.067M cacodylate buffer (pH 7.4), post-fixed in a mixture of 1% osmium tetraoxide and 1.5% potassium ferrocyanide, and then embedded in epoxy resin (Taab). The ultrathin sections were examined under a TEM (Hitachi H-7000, Hitachi).

Immunohistochemistry

Serial sections were incubated with anti-Runx2 monoclonal antiboby (MBL), processed with Histofine Simple Stain MAX-PO(M) (Nichirei), and treated with phosphate buffer containing 0.05% 3,3′-diaminobenzidine(DAB), 0.01% nickel chloride, and 0.01% H_2O_2. For double labeling, the sections were incubated with rabbit anti-mouse osteocalcin polyclonal antibody (Takara) or rabbit anti-mouse osteopontin polyclonal antibody (IBL), processed with Histofine Simple Stain MAX-PO(R) (Nichirei), and treated with phosphate buffer containing 0.05% DAB and 0.01% H_2O_2. The sections were counterstained with methyl green.

In Vitro Osteoclastogenesis

Bone marrow cells were obtained from the tibias and femurs of 4- to 6-week-old C57BL/6 male mice, and primary osteoblastic cells were prepared from calvariae of C57BL/6 newborn mice. The osteoblastic cells were infected with EGFP-, *Runx2*-and-EGFP-, or dn-*Runx2*-and-EGFP-containing adenovirus. Bone marrow cells (5×10^5/ml) and osteoblastic cells (5×10^4/ml) were co-cultured in 200 μl α-MEM containing 10% heat-inactivated FBS in the presence of 10^{-8} M 1α, 25-dihydroxyvitamin D_3 [1α, $25(OH)_2D_3$] (Wako) and prostaglandin E_2 (10^{-6} M) (Wako) on 96-well plates for 6 days. Media were changed every other day. Osteoclast formation was evaluated by TRAP staining. Cultured cells were fixed with 4% paraformaldehyde for 30 min, washed in 0.2% Triton X-100 at room temperature for 5 min, and incubated in acetate buffer (pH 5.0) containing naphthol AS-MX phosphate (Sigma), fast red-violet LB salt (Sigma), and 50 mM sodium tartrate. For the evaluation of bone resorption, the bone marrow cells and osteoblastic cells were co-cultured on dentin slices (Wako) for 6 days, the slices were stained with Coomassie Brilliant Blue R, and the resorbed area was analyzed using NIH image software.

PTH Administration and Micro-CT Analysis

Rat PTH(1-34) (Sigma) was administered to experimental animals subcutaneously as three injections per day over 8 hr at a dose of 80 μg/kg (total 240 μg PTH/kg/day) for 18 days. Control animals were given vehicle alone. Animals were then sacrificed and bone samples were collected to study trabecular bone mass and micro-architecture. Quantitative micro-computed tomography (micro-CT) was performed with a micro-CT system (μCT-20; Scanco Medical). Data from scanned slices was used for three-dimensional analysis to calculate femoral morphometric parameters, including trabecular and cortical bone volume density (bone volume [BV]/tissue volume [TV]), trabecular thickness (Tb.Th = 2 × BV/bone surface [BS]) and trabecular number [Tb.N = (BV/TV)/Tb.Th]. Trabecular bone parameters were measured on distal femoral metaphysis. Approximately 4.8 mm (0.5 mm far from the growth plate) were cranio-caudally scanned and a total of 400 slices with 12-μm increments were taken. Cortical BV/TV was measured on femoral diaphysis and proximal metaphysis.

Statistical Analysis

Statistical analyses were performed using a Student's *t*-test. $P < 0.05$ was considered to be significant.